Experimental and Analytical of Ultrasonic Elliptical Vibration Cutting of Micro-pyramid Reflective Mold Based on Guided Wave Transmission

Tao Jiang (jiangtao@jmu.edu.cn)
Jimei University https://orcid.org/0000-0002-2967-5891
Jintao Yang
Jimei University
Jun Pi
Jimei University
Wenyu Luo
Jimei University
Jun Zhang
Jimei University

Research Article

Keywords: Ultrasonic elliptical vibration cutting, Guided wave transmission, Deflection angle, Microstructure, Elliptic trajectory

Posted Date: March 9th, 2021

DOI: https://doi.org/10.21203/rs.3.rs-275009/v1

The International Journal of Advanced Manufacturing Technology manuscript No.
(will be inserted by the editor)

Experimental and Analytical of Ultrasonic Elliptical Vibration Cutting of Micro-pyramid Reflective Mold Based on Guided Wave Transmission

Tao Jiang · Jintao Yang · Jun Pi · Wenyu Luo · Jun Zhang

Received: date / Accepted: date

Abstract The ultrasonic elliptical vibration cutting (UEVC) technique has been found to be a promising technique for ultraprecision machining of microstructural functional surfaces. However, the current UEVC technique can't achieve higher frequency ultrasonic cutting due to its rigid orthogonal vibration transmission. To further study the cutting mechanism and removal characteristics in high frequency UEVC of microstructural surface, the UEVC based on flexible guided wave transmission is proposed which can achieve 96.8 kHz. The influence of bending vibration of guided wave band on longitudinal vibration is elaborated with the model of the bending vibration dynamic model of the guided wave. The model of elliptical trajectory deflection of tool tip is established. Based on the theoretical modeling and finite element simulation, the residual height and material removal characteristics of elliptic trajectory with variable deflection angle are simulated and analyzed. The results show that when the deflection angle is between 10° and 70°, the tangential force is small and stable. Finally, the cutting experiments of micro-pyramid reflective mold in guided wave UEVC and conventional cutting (CC) are carried out. Compared with CC, high-frequency UEVC can obtain micro-pyramid elements with average roughness of 5.21 nm, that verifies the applicability of high-frequency UEVC in precision machining of microstructure.

Keywords Ultrasonic elliptical vibration cutting · Guided wave transmission · Deflection angle · Microstructure · Elliptic trajectory

Tao Jiang
College of Mechanical and Energy Engineering, Jimei University, No.9 Shigu road, Xiamen, Fujian province, China
Tel.: +86-0592-6183521
E-mail: jiangtao@jmu.edu.cn

Jintao Yang
College of Mechanical and Energy Engineering, Jimei University, No.9 Shigu road, Xiamen, Fujian province, China
E-mail: 18855037848@163.com

Jun Pi
College of Mechanical and Energy Engineering, Jimei University, No.9 Shigu road, Xiamen, Fujian province, China
E-mail: pi_jun@163.com

Wenyu Luo
College of Mechanical and Energy Engineering, Jimei University, No.9 Shigu road, Xiamen, Fujian province, China
E-mail: 202011802012@jmu.edu.cn

Jun Zhang
College of Mechanical and Energy Engineering, Jimei University, No.9 Shigu road, Xiamen, Fujian province, China
E-mail: 1310722389@qq.com

1 Introduction

With the development of science and technology products towards high performance, high precision and high integration, microstructural functional surfaces have attracted extensive attention and research due to their advantages in mechanical, physical, chemical properties and easy integration [1–3]. The ultra-precision microstructure function surface mold is mainly manufactured by ultra-precision turning, ultra-precision grinding, chemical etching, energy field assisted machining and so on [4, 5]. In contrast, ultra-precision cutting technology is an important method to manufacture the microstructure surface mold because of its high machining deterministic, high accuracy surface and wide applicability. In the past precision cutting process, the material removal characteristics change obviously when the depth of cutting is increased [6]. The workpiece is easy to produce defects such as residual stress, tear and burr, which cause serious tool wear, affect the profile accuracy and surface roughness of the machined surface, and then restrict their application and development.

To improve the machining accuracy of microstructure surface mold, UEVC technology is introduced as the main manufacturing method. UEVC technology was first proposed and developed by Shamoto and Moriwaki [7, 8]. Two groups of PZT plates are arranged symmetrically on the four faces of the column horn, and the excitation voltage with specific phase difference is applied to make the horn produce the same frequency first-order bending resonance mode, and the two bending vibrations are overlayed to form the elliptical trajectory of the tool tip. Then the improved elliptical vibration cutting device with third order resonant mode by them [9]. Since then, based on the theory of elliptical vibration cutting, many scholars have proposed and set up the elliptical vibration cutting device such as longitudinal-bending resonance type [10], rigid orthogonal excitation type [11] and Langevin type [12], etc.

Compared with conventional cutting, because of the elliptical vibration of the tool tip, the contact and separation between the tool and the workpiece are strengthened, the effect of ultrasonic cutting is increased, the cutting force of the tool is improved, and the lubrication and cooling efficiency of the cutting process are improved [13, 14]. To further study the cutting mechanism and material removal characteristics of elliptical vibration cutting, scholars have carried out various research based on the elliptical vibration cutting device [15–17]. Shamoto found that the cutting depth and speed of the tool are always changing in the process of elliptical vibration cutting, and put forward the mathematical model of transient tool position, average shear angle and transient cutting force [7]. Based on the comprehensive analysis of TOC (thickness of cut), transient shear angle and transient reversal friction, Zhang established the analytical model of cutting force for orthogonal elliptic vibration cutting and verified the accuracy of the model through experiments [18]. Jiang realizes high-speed intermittent ultrasonic vibration cutting by using phase control, which can effectively reduce cutting force by 20% - 50%, increase tool life by 1.5-3.0 times, and the machining efficiency can be increased by 90% [19]. Kim studied the characteristics of elliptical vibration cutting in micro V-grooving by using orthogonal piezoelectric ceramic transducers. It is found that the separation and contact between tool and workpiece was the prerequisite to realize the advantages of EVC [20–22]. In EVC, the cutting force is significantly reduced, and the excitation frequency or acceleration slightly increased [23–25].

As the UEVC system has a special tool tip trajectory, and the excitation frequency of the cutting system is generally concentrated in 20-50 kHz, the cutting speed is limited and the machining efficiency is low [26–28]; however, the high-frequency UEVC system has some shortcomings such as complex structure design, difficult coupling of vibration transmission, poor trajectory control accuracy, etc., which lead to the removal of high-frequency UEVC technology are few reports on the cutting characteristic in microstructure surface mold. Therefore, in the present research, a high-frequency UEVC device with the resonant frequency of approximately 100 kHz is built by using the guided wave band to transmit vibration, and two longitudinal vibration transducers are set up to excite the longitudinal and bending vibration modes of cutting tools. Based on the flexible guided wave propagation, the orthogonal excitation vibration coupling model is established, and the finite element simulation of the influence of elliptic trajectory deflection on the cutting process is carried out. Finally, guided wave UEVC device is applied to machine micro-pyramid reflective mold, and cutting experiments are carried out to verify the ultra-precision machining ability of high frequency guided wave UEVC technology.

2 Principle of Elliptical Vibration Cutting

In elliptical vibration cutting, two orthogonal transducers with phase shift or resonant transducers are often used to excite the tool to produce vibration in two directions at the same time. The principle of elliptical vibration cutting is shown in Fig.1. The diamond tool moves along the x-axis direction, and each cutting cycle can be divided into four processes: first, the tool starts cutting from point A on the previous machined surface and reaches the bottom point B, and the workpiece is compressed downward by the tool and elastic deformation occurs; secondly, the tool moves from point B through point C to reversal friction point D. The vibration velocity of rake face along horizontal direction is less than that of chip flow, and the chip is compressed downward by friction force, which is consistent with the conventional cutting process; at point E, the friction force between the rake face and the chip becomes zero. Then, the tool moves from point E to point F, as the velocity of the rake face in the horizontal direction is less than the flow velocity of the chip in this process, the friction force changes reversal direction, and the chip is pulled up by the friction force. Finally, the tool separates from the workpiece at point F and enters the next cutting cycle, and the chip is no longer subject to friction. When the chip is subjected to reverse friction, the average friction force in the whole cutting cycle could be less than zero. The elliptical vibration of the tool will also change the shear angle of the contact area between the tool and the workpiece. At the same time, due to the separation of the tool and the workpiece, it is helpful to achieve better cutting lubrication.

When the tool moves along the negative direction of x-axis with the cutting speed of v and the angular frequency of ω, the motion trajectory of the tool tip is as follows:

$$\begin{cases} x(t) = a\cos\omega t - vt \\ y(t) = b\cos(\omega t + \phi) \end{cases} \tag{1}$$

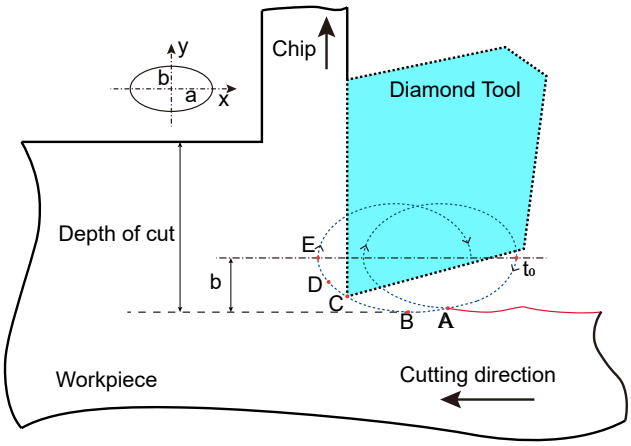

Fig. 1 Elliptical vibration cutting process

Where a and b are the tangential and normal amplitudes of cutting vibration respectively, and the phase shift of the orthogonal vibration excitation is ϕ.

3 Guided Wave Ultrasonic Elliptical Vibration Cutting Technology

3.1 Guided Wave Ultrasonic Elliptical Vibration Cutting Device

In order to improve the precision machining quality of micro-pyramid reflective mold, an orthogonal elliptical vibration cutting device based on guided wave transmission technology is proposed. Fig.2(a) shows a schematic illustration of the guided wave elliptical vibration cutting device whose resonant frequency is approximately 100 kHz. The device consists of dual channel ultrasonic generator (DCUG), full wavelength longitudinal vibration transducer (FWLVT), guided wave band (GWB), tool head (TH) and single crystal diamond tool (SCDT). The two full wavelength transducers are excited by high frequency sinusoidal excitation with the same frequency and a certain phase shift through a dual channel ultrasonic generator to generate the longitudinal vibration of the full wavelength transducer. The guided wave band with weak coupling in non-transmitting direction is used to transmit the vibration. Wherein, the longitudinal mode of tool head is excited by the guided wave band of y direction and bending mode of tool head is excited by guide wave band of x-direction. By combining the two resonant vibrations, the diamond tool tip forms an elliptic trajectory. Fig.2(b) shows the harmonic response simulation analysis of the device with FEA. According to the simulation results, the resonance frequency of the device is 99.4 kHz.

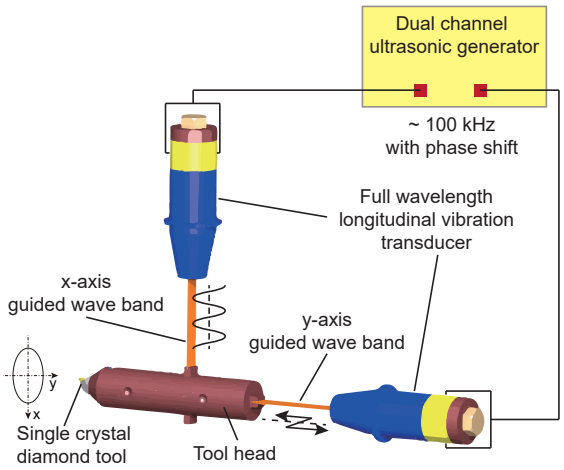

(a) Schematic diagram of the orthogonal guided wave UEVC device

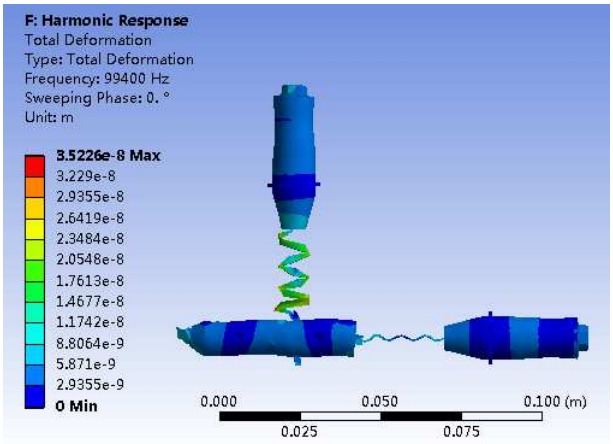

(b) Harmonic response simulation of the guided wave UEVC device

Fig. 2 Guided wave UEVC device

3.2 Influence of Bending Vibration of Guided Wave Band on Longitudinal Vibration

The guided wave band is a kind of vibration transmission medium, which makes the longitudinal wave or transverse wave in the guided wave band reflect back and forth on the parallel boundary and travel along the direction of the parallel plate surface to complete the guided wave transmission. The typical structures of the guided wave band are cylindrical and plate-shaped, which can excite longitudinal mode and multi-order bending mode in the process of guided wave transmission. The cross-section of single guided wave band is small, and the acoustic load impedance is exceedingly small, which makes it has good unidirectional dynamic stiffness characteristics. At the same time, due to its flexible structure, it has weak coupling characteristics in the non-transmission direction, which makes the transmission coupling efficiency of the orthogonal guided wave bands higher. For the UEVC device with orthogonal excitation, when rigid

structure coupling is adopted, there is a large vibration interference of orthogonal excitation, which influences the natural frequency and the main mode of vibration mutually, and finally leads to a big elliptic trajectory error at the tool tip; the guided wave transmission can avoid the orthogonal coupling error and improve the coupling quality of the vibration system. As shown in Fig.2, the guided wave UEVC device is driven by two longitudinal vibration mode guide wave bands. Therefore, it is necessary to avoid the high-frequency bending vibration mode generated by the guided wave bands, so as to reduce the impact on the coupling efficiency of longitudinal vibration transmission. In addition, the transmission of longitudinal vibration generated by full wavelength longitudinal vibration in guided wave band will be affected by bending vibration due to the Poisson effect.

In order to explore the mutual influence and impedance frequency characteristics of orthogonal guided wave transmission, it is necessary to establish the differential equation of guided wave band bending vibration. First, the following assumptions are made to simplify the analysis:

(1) The central principal axis of each section of the guided wave band are in the same plane, and the transverse vibration occurs in this plane.

(2) The cross section of the guided wave band is much smaller than its length, so the influence of moment of inertia and shear deformation can be ignored.

(3) The transverse vibration of the guided wave band is in accordance with the assumption of small deflection plane bending, that is, the amplitude of transverse vibration is small in the linear range.

According to the hypothesis, the transverse free vibration model of guided wave band is established, as shown in Fig.3. The cross-section area of the guided wave band is s, the mass of unit length is m, the density is ρ, the moment of inertia of the cross-section is I, and the bending strength of the cross-section is EI. The shear force and bending moment of the micro element dx at the cross-section x of the guided wave band are Q and M respectively.

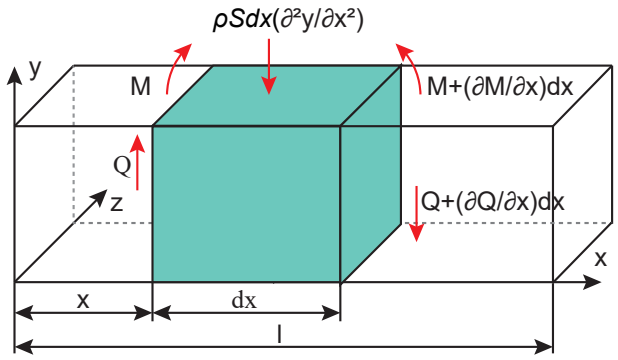

Fig. 3 Transverse free vibration model of guided wave band

According to D'Alembert's principle, the inertial force generated by the micro element dx can be expressed as:

$$Q-\left(Q+\frac{\partial Q}{\partial x}dx\right)-\rho Sdx\frac{\partial^2 y}{\partial t^2}=0 \tag{2}$$

The equation can be simplified as:

$$\frac{\partial Q}{\partial x}=-\rho S\frac{\partial^2 y}{\partial t^2} \tag{3}$$

Similarly, according to the mechanics of materials, any point on the right side of the micro element dx is taken as the moment balance equation, and then

$$\frac{\partial Q}{\partial x}=\frac{\partial^2 M}{\partial x^2}=\frac{\partial^2}{\partial x^2}\left(EI\frac{\partial^2 y}{\partial x^2}\right)=EI\frac{\partial^4 y}{\partial x^4} \tag{4}$$

By substituting the equation 4 into equation 3, the equation of motion for transverse free vibration of the guided wave band with uniform section can be obtained:

$$\frac{\partial^4 y}{\partial x^4}=-\frac{1}{a^2}\frac{\partial^2 y}{\partial t^2} \tag{5}$$

Where $a=\sqrt{\frac{EI}{\rho S}}$. Therefore, the mode function of transverse free vibration of the guided wave band can be expressed as:

$$Y(x)=A\sin\lambda x+B\cos\lambda x+C\,\mathrm{sh}\,\lambda x+D\,\mathrm{ch}\,\lambda x \tag{6}$$

Where A, B, C, D is the boundary parameter. After introducing the Krylov function, the above equation can be expressed as follows:

$$Y(x)=C_1S(\lambda x)+C_2T(\lambda x)+C_3U(\lambda x)+C_4V(\lambda x) \tag{7}$$

When the longitudinal vibration transducer and tool head are connected by the guided wave band, one end of the longitudinal vibration transducer is fixed, and the other end of the tool head is free. The boundary condition of the guided wave band is that one end is fixed and the other end is free:

$$\begin{cases} C_1=C_2=0 \\ C_3S(\lambda l)+C_4T(\lambda l)=0 \\ C_3V(\lambda l)+C_4S(\lambda l)=0 \end{cases} \tag{8}$$

As a result:

$$\begin{vmatrix} S(\lambda l) & T(\lambda l) \\ V(\lambda l) & S(\lambda l) \end{vmatrix}=0 \tag{9}$$

The approximate mathematical expression of non-zero roots can be obtained by graphic method:

$$\lambda_1 l=1.875\lambda_2 l=4.694\lambda_i l\approx\frac{2i-1}{2}\pi(i=3,4\cdots) \tag{10}$$

Then, the natural frequency of transverse vibration of guided wave band is

$$\omega_{ni}=\left(\frac{2i-1}{2l}\pi\right)^2\sqrt{\frac{EI}{\rho S}}(i=1,2,\cdots) \tag{11}$$

In the same way, the modal function of transverse vibration of guided wave band can be obtained as:

$$Y_i(x) = \cos\lambda_i x - \mathrm{ch}\,\lambda_i x + \frac{\cos\lambda_i l + ch\lambda_i l}{\sin\lambda_i l + \mathrm{sh}\,\lambda_i l}(\sin\lambda_i x - \mathrm{sh}\,\lambda_i x) \tag{12}$$

Fig.4 is the four-order bending modes of the guided wave band UEVC device. When the guided wave band is in the τth order bending vibration (transverse vibration), there will be $\tau + 1$ bending vibration displacement points. Generally, the bending vibration produced by UEVC device is less than the fifth order.

When the guided wave band is a plate-shaped, the inertia

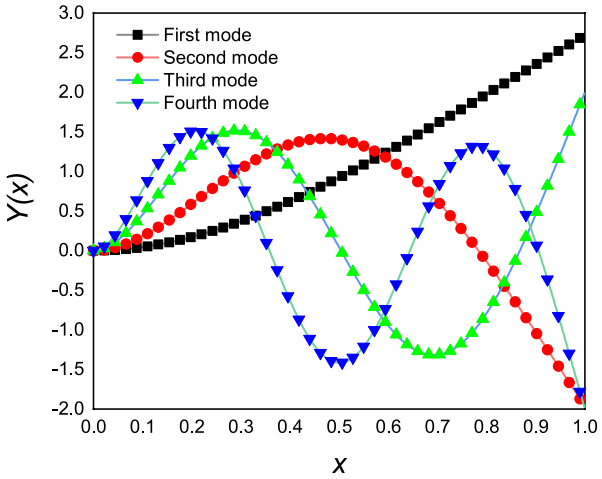

Fig. 4 Bending mode of guided wave band in orthogonal UEVC device

moment I of the cross-section to the central principal axis is:

$$I = \frac{bh^4}{12} \tag{13}$$

Where b is the width of the plate-shaped guided wave band and h is the thickness of the plate-shaped guided wave band. By substituting equation 13 into equation 11, it is found that the thickness h is the main factor affecting the bending vibration fundamental frequency of the plate-shaped guided wave band. Fig.5 shows the relationship between the order of the plate-shaped guided wave band and the bending vibration fundamental frequency.

It can found that the higher the order is, the more significantly the bending vibration fundamental frequency of the plate-shaped guided wave band will increase; when the lower thickness of the guided wave band is used, the bending vibration fundamental frequency can be significantly reduced. Therefore, the design of plate-shaped guided wave band follows the following two principles:

(1) The lower thickness should be chosen as far as possible

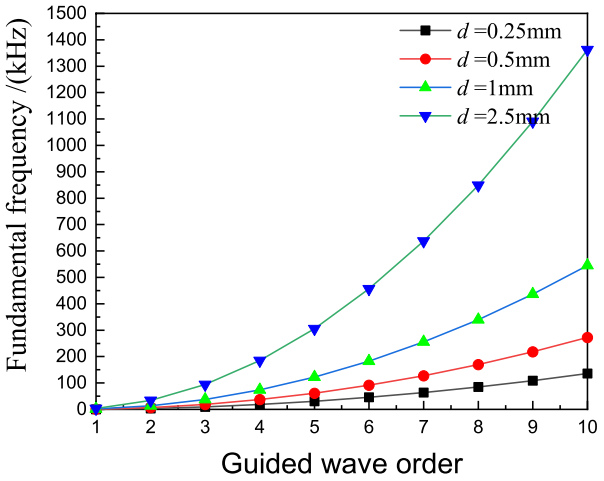

Fig. 5 The relation between the order of the plate-shaped guided wave band and the fundamental frequency of bending vibration

to ensure the UEVC device is reasonable when selecting the plate-shaped guided wave band.

(2) The bending vibration of UEVC device should be selected at the low order, so that the fundamental frequency of its bending vibration is far less than the resonant frequency of the system.

Based on the above analysis, for the UEVC device of which resonant frequency is approximately 100 kHz, when the longitudinal vibration transducers are excited in orthogonal direction at the same time, the bending vibration generated by one directional transducer has almost negligible influence on the longitudinal vibration generated by the other directional transducer in guided wave UEVC device. The two longitudinal vibration transducers can transmit the longitudinal vibration independently through the guided wave band, obtained good coupling effect.

3.3 Modelling of The Tool Tip Elliptic Trajectory Deflect

In elliptic vibration cutting, elliptic trajectories with different positions can be formed by controlling of trajectory motion parameters, which will affect the machining surface quality, tool wear and cutting residual height. For orthogonal UEVC device, the motion parameters of tool tip elliptic trajectory mainly include amplitude, phase shift and deflection angle. In the tool tip elliptic trajectory motion parameter, the control of amplitude and phase shift only needs to adjust the excitation voltage and the phase shift of input excitations, while the control of deflection angle needs to ensure the same shape and different deflection angle of the tool tip elliptic trajectory, the essence of which is coordinate transformation around the center of the elliptic trajectories.

The elliptic trajectory deflection model of the tool tip is shown in Fig.6, the elliptic trajectory of the tool tip in the

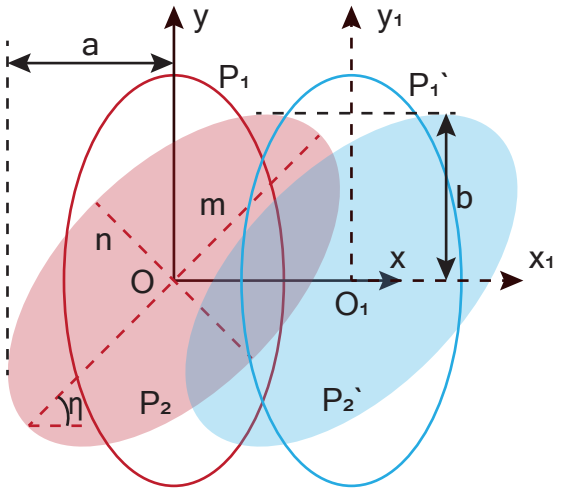

Fig. 6 Tool tip elliptic trajectory deflection model

Oxy plane is transformed from P_1 to P_2, and the deflection angle is τ; Similarly, the tool tip elliptic trajectory $P_1^{`}$ in $O_1x_1y_1$ plane is transformed into $P_2^{`}$. In Oxy plane, the amplitudes of the tool tip elliptic trajectory after deflection are a and b, while the amplitudes n and m relative to its major axis and minor axis remain constant with the variation of deflection angle η.

When the tool tip moves from P_1 to $P_1^{`}$ in continuously cutting, the motion equation of the tool tip elliptic trajectory relative to the workpiece is

$$\begin{cases} x(t) = m\sin(2\pi ft + \theta) + vt \\ y(t) = n\cos(2\pi ft) \end{cases} \tag{14}$$

Where, θ is the phase shift before deflection; f is the resonant frequency; v is the cutting speed. When the tool tip elliptic trajectory deflects around the center of the ellipse, the coordinates after rotation can be expressed as follow:

$$\begin{bmatrix} x'(t) \\ y'(t) \end{bmatrix} = \begin{bmatrix} \cos\eta & -\sin\eta \\ \sin\eta & \cos\eta \end{bmatrix} \begin{bmatrix} x(t) \\ y(t) \end{bmatrix} \tag{15}$$

By combining the above two equations, the amplitude a, b and phase shift β of the tool tip elliptic trajectory P_2 after deflection in Oxy plane are obtained, which is:

$$\begin{cases} a = \sqrt{m^2\cos^2\eta + n^2\sin^2\eta} \\ b = \sqrt{m^2\sin^2\eta + n^2\cos^2\eta} \\ \beta = \arccos\left[\frac{m\cos\eta}{\sqrt{m^2\cos^2\eta + n^2\sin^2\eta}}\right] - \operatorname{acrsin}\left[\frac{m\sin\eta}{\sqrt{m^2\sin^2\eta + n^2\cos^2\eta}}\right] \end{cases} \tag{16}$$

According to the amplitude m, n and deflection angle η, the amplitude a, b and phase shift β after deflection are solved, and the result is shown in Fig.7.

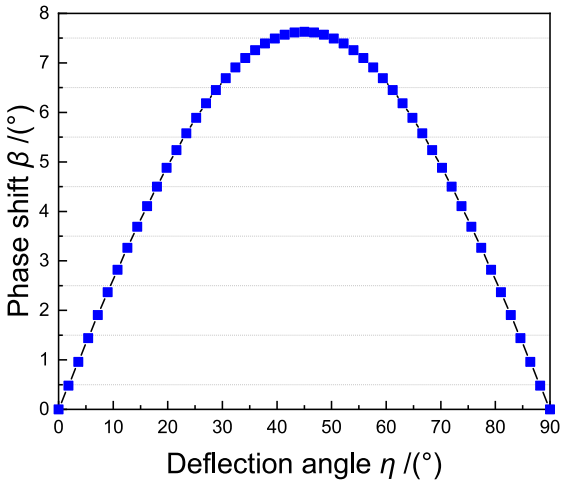

(a) The relationship between deflection angle and phase shift after deflection

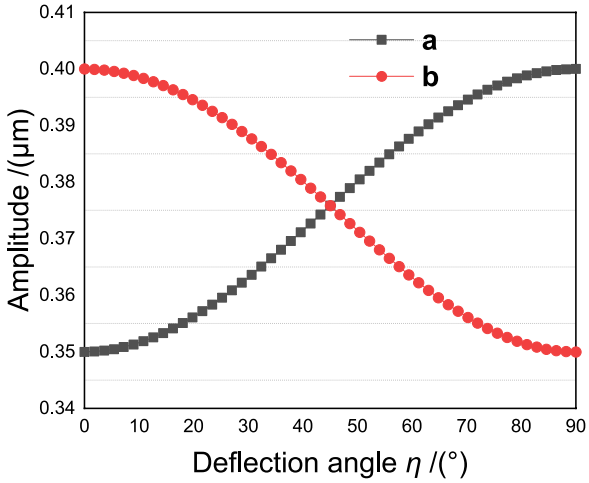

(b) The relationship between deflection angle and amplitude after deflection

Fig. 7 The relationships between deflection angle and phase shift and amplitude

3.4 Modelling of The Elliptic Trajectory Cutting Residual Height

The most intuitive performance of the machining surface is the cutting residual height due to the difference of the tool tip ellipse trajectory. Shamoto deduced a mathematical model between the cutting residual height and the longitudinal amplitude, frequency and phase shift [7]. Kim proposed another calculation method [20], which shows that the residual height is directly proportional to the square of the longitudinal amplitude and relative cutting speed, and inversely proportional to the square of frequency and of the transverse amplitude. The calculation model of the residual height of elliptic trajectory is shown in Fig.8.

The ellipse in Oxy plane is the tool tip trajectory of the current cycle; the ellipse in the $O_1x_1y_1$ plane is the tool tip trajectory of the next cycle. According to the elliptic shape,

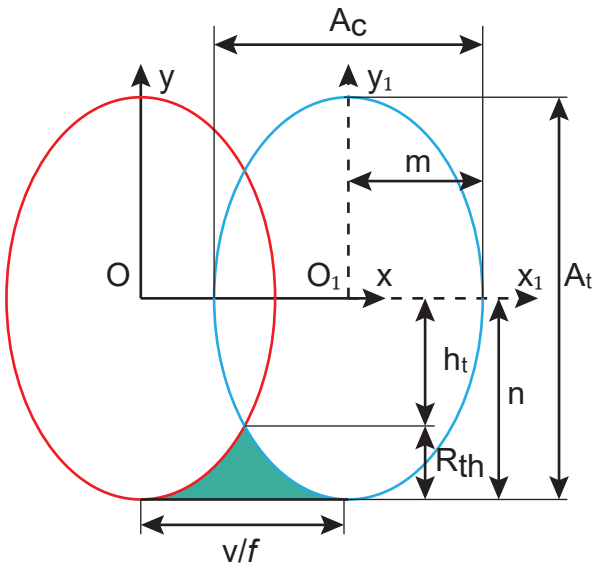

Fig. 8 Model of the residual height of elliptic trajectory

the model is as follows:

$$\begin{cases} h_t = \left(\frac{A_t}{2}\right)\sqrt{1-\left(\frac{v}{fA_c}\right)^2} \\ R_{th} = \left(\frac{A_t}{2}\right)\left(1-\sqrt{1-\left(\frac{v}{fA_c}\right)^2}\right) \end{cases} \tag{17}$$

Where, h_t is the distance between the intersection point of the elliptic trajectory of the two periodic tool tips and the x-axis; A_t is twice the amplitude n in y-axis; A_c is two times the amplitude m in x-axis. To achieve the separation of tool and workpiece, speed ration (SR, the ratio of cutting speed to maximum vibration speed) should be less than 1. As SR is less than 1, fA_c/v is greater than 1. By means of the Taylor series transformation, the residual height is approximately as:

$$R_{th} \approx \left(\frac{A_t}{4}\right)\left(\frac{v}{fAc}\right)^2 \tag{18}$$

Considering the influence of tool tip elliptic trajectory deflection, the equation 16 is substituted into equation 18 to obtain the residual height model of variable deflection angle tool tip ellipse trajectory:

$$\begin{aligned} R_{th} &= \frac{1}{4}\left(\frac{A_t}{A_c^2}\right)\left(\frac{v}{f}\right)^2 = \frac{1}{8}\left(\frac{b}{a^2}\right)\left(\frac{v}{f}\right)^2 \\ &= \frac{1}{8}\left(\frac{\sqrt{m^2\sin^2\eta + n^2\cos^2\eta}}{m^2\cos^2\eta + n^2\sin^2\eta}\right)\left(\frac{v}{f}\right)^2 \end{aligned} \tag{19}$$

The relationship between deflection angle and residual height is obtained as shown in the Fig.9.

When the deflection angle increases, the residual height decreases first and then increases; when the deflection angle is 90°, the residual height is the minimum. In practical UEVC machining, the residual height is also affected by cutting force and cutting angle.

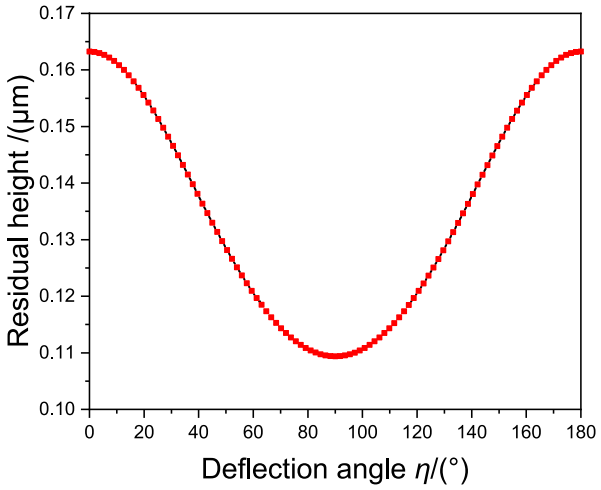

Fig. 9 Relationship between the residual height and the deflection angle of elliptic trajectory

3.5 Resonance Frequency and Tool Tip Elliptic Trajectory Test of The Guided Wave UEVC Device

Based on the above guided wave band transmission theory and tool tip trajectory analysis, the UEVC device is shown in Fig.10 after the parts are precisely manufactured and assembled. In order to test the resonant frequency of the UEVC device and verify the cutting ability and the controllability of the tool tip elliptic trajectory of the orthogonal guided wave UEVC system, impedance analyzer (ZX-70A-200khz) and Doppler laser vibrator (NLV-2500) are used to detect and analyze the resonant frequency of the system and the tool tip motion trajectory.

The test result shows in Fig.11. According to the test, the resonant frequency of the longitudinal mode F_s is 96.86 kHz, and the anti-resonant frequency F_p is 101.78 kHz; the resonant frequency of bending mode F_s is 96.83 kHz, and the anti-resonant frequency F_p is 102.38 kHz. The difference of the resonant frequency of the two directions is 0.03%, indicating that the UEVC device can achieve the same frequency excitation in orthogonal directions. The results of the laser vibrometer show that the amplitude in orthogonal directions of the tool tip is 0.55 μm and 0.46 μm respectively at the initial voltage of 3 V and amplification of 38 times. By changing the phase shift, the elliptic trajectory of the actual tool tip is partially deformed, but it is still deflected with the phase shift, which has a good consistency in general, indicating that the UEVC system can achieve higher response accuracy, controllability and stability.

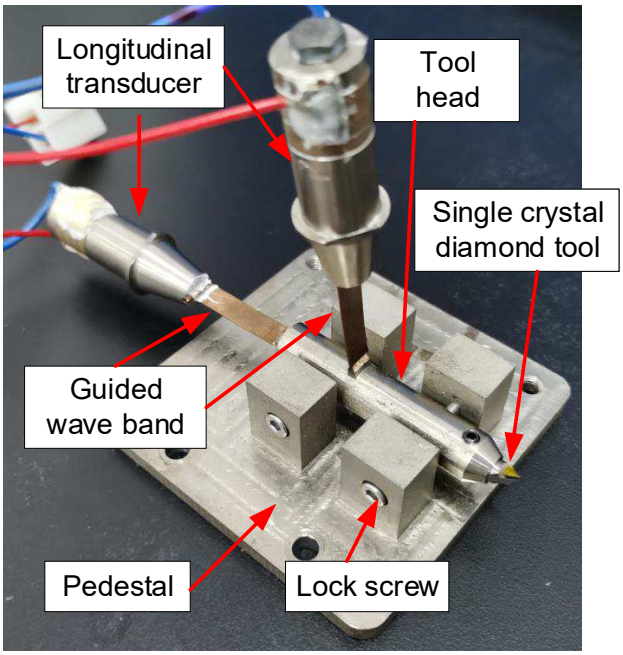

(a) The guided wave UEVC device

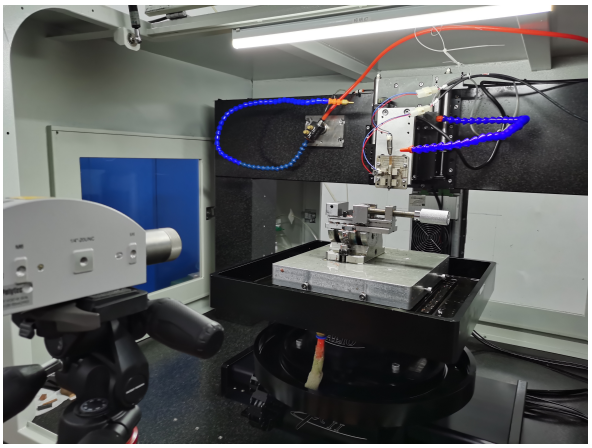

(b) Test of resonant frequency and amplitude with laser vibrometer

Fig. 10 The guided wave UEVC device and the test of resonant frequency and amplitude

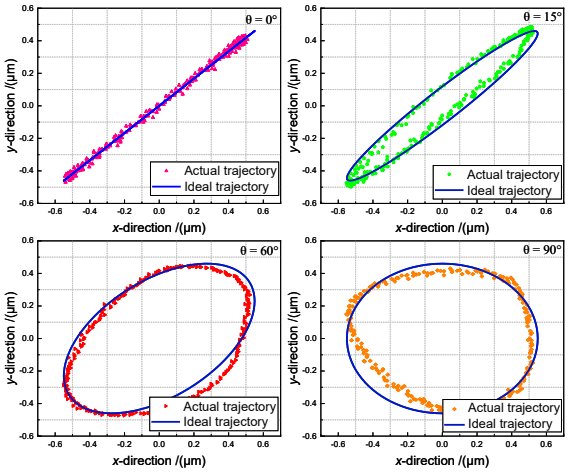

Fig. 11 The elliptic trajectory of the guided wave UEVC device

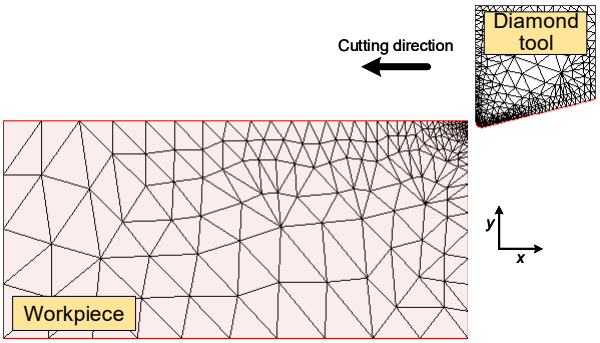

Fig. 12 FEA model of the UEVC

4 Simulation of Ultrasonic Elliptical Vibration Cutting

4.1 Model of The Ultrasonic Elliptical Vibration Cutting

The FEA method is applied to simulate the elliptic trajectory of the tool tip with variable deflection angle, the cutting force, tool temperature, chip and surface morphology in UEVC, so as to further explain the UEVC cutting mechanism and obtain the optimized surface machining parameters. The cutting model is shown in Fig.12. The analysis process is as follows: first, micro-machining process was adopted (suitable for cutting with the resonant frequency 100 kHz and the amplitude less than 1 μm); secondly, the workpiece geometry and material Settings, the material is chosen C77700Brass(US); the tool size and the material, which is Single Crystal Diamond, and the mechanical and thermal boundary conditions are defined; then, the cutting parameters are set (cutting depth, feed, cutting speed, etc.); finally submit the calculation. The simulation parameters are shown in Table 1.

Table 1 Simulation parameters

Parameters	Unit	Value
Rake angle	°	0
Relief angle	°	14
Tool radius	μm	0.2
Initial temperature	°C	20
Resonant frequency	kHz	100
Vibration Amplitude m	μm	0.35
Vibration Amplitude n	μm	0.4
Phase shift θ	°	90
Cutting depth	μm	0.6
Cutting speed	mm/s	50

4.2 Analysis of The Cutting Force and Temperature of The UEVC With Varied Deflection Angle

Fig.13 shows the cutting force and tool temperature analysis of UEVC with variable deflection angle, the model used in simulation changes from vertical elliptic trajectory (VET) to horizontal elliptic trajectory (HET).

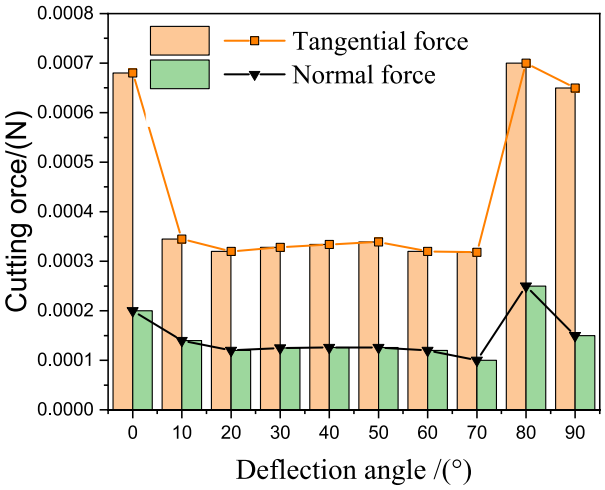

(a) Average cutting force

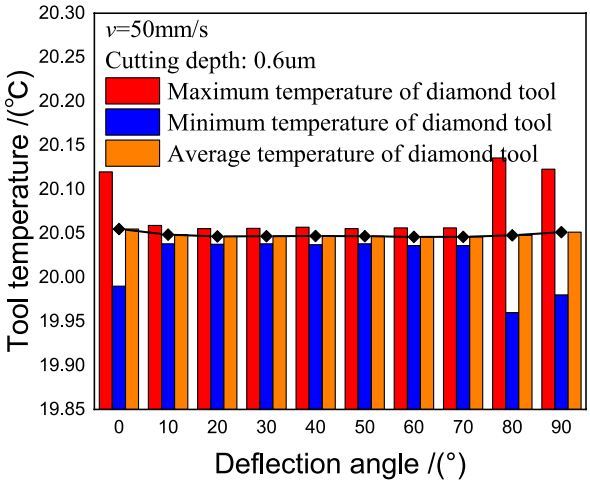

(b) Tool temperature

Fig. 13 Simulation of the cutting force and temperature of the tool in UEVC with variable deflection angle

When VET changes to HET, the deflection angle η increases from 0° to 90° and the tangential force is more than twice of the normal force, indicating that the tangential force is always the dominant force for chip removal in UEVC with variable deflection angle, which is different from that in UEVC with variable phase shift [29]. When η is between 10° and 70°, the average cutting force is relatively stable; at about 20° and 70° the cutting force decreases, and after 70° rises obviously. HET (η = 90°) is a typical tool tip elliptic trajectory, which reduces the sharpness of the tool. Although it can reduce the impact force, it also increases the cutting force. The trend of tool temperature is consistent with the law of cutting force, but the change of tool temperature is not so obvious.

4.3 Analysis of The Chip of UEVC With Varied Deflection Angle

Fig.14 shows the analysis of chip by UEVC with variable deflection angle. In Fig.14(a), with the increase of deflection angle, the chip is in strip shape, which is mainly concentrated between the deflection angle of 20° and 70°. The result shows that, because of the small change of cutting force, the cutting process is more stable, so it is easier to get better surface quality.

In Fig.14(b), when the deflection angle is 0° and 90°, the chip thickness is basically the same, but the chip status is different. The chips of 90° deflection angle (HET) become smaller spiral curvature, indicating that the sharpness of the tool is lower, less impact, more suitable for brittle materials processing; The chips of 0° deflection angle (VET) turn into larger spiral-shaped curvature, indicating a higher sharpness of the tool, and the friction reversal effect is more obvious. It is more suitable for the processing of high hardness materials, so as to obtain continuous and smooth chips and avoid secondary damage to the processed surface caused by chip breakage.

4.4 Simulation Comparison Between UEVC and CC

In order to compare the trend of cutting force in UEVC and CC, the simulations of the influence of different cutting depth and cutting speed on cutting force are carried out. The analysis results are shown in Fig.15. According to the Fig.15(a), the cutting force increases with the increase of cutting depth. The cutting force of UEVC is far less than that of CC, and the tangential cutting force is about twice of normal cutting force. When the cutting depth changes, the cutting force caused by the change of phase shift also fluctuates. When the cutting depth is less than 0.5 μm, the cutting force with phase shift of 90° is the minimum; when the cutting depth is 0.5 μm to 1 μm, the cutting force with phase shift of 60° is less than 90°; when the cutting depth is greater than 1 μm, the cutting force increases significantly; when the cutting depth is greater than 3 μm, the influence of phase shift decreases; when the cutting depth is greater than 0.5 μm, the cutting force with phase shift of 120° is always kept the minimum; until the cutting depth is 3 μm, the influence of phase shift will be reduced.

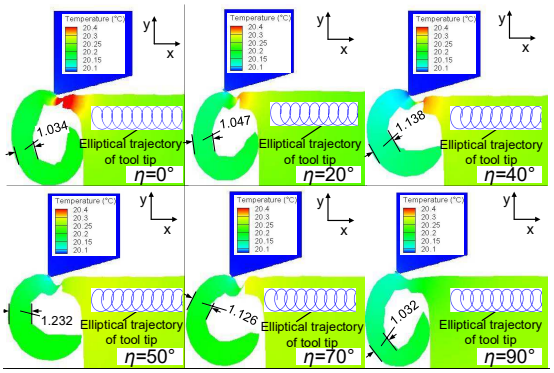

(a) The morphology of the UEVC with varied deflection angle

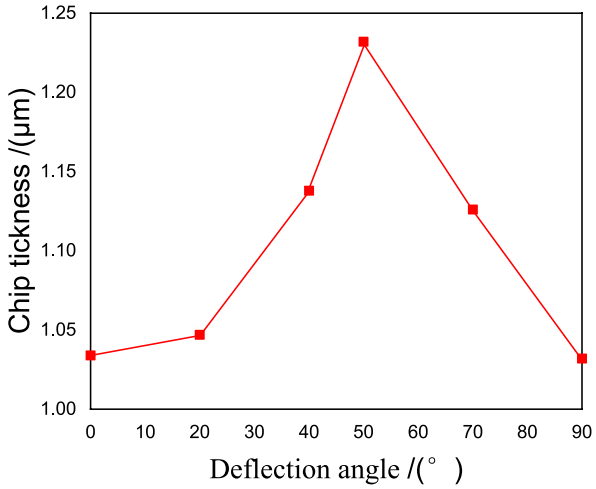

(b) The chip thickness of the UEVC with varied deflection angle

Fig. 14 Simulation of the chips of the UEVC with varied deflection angle

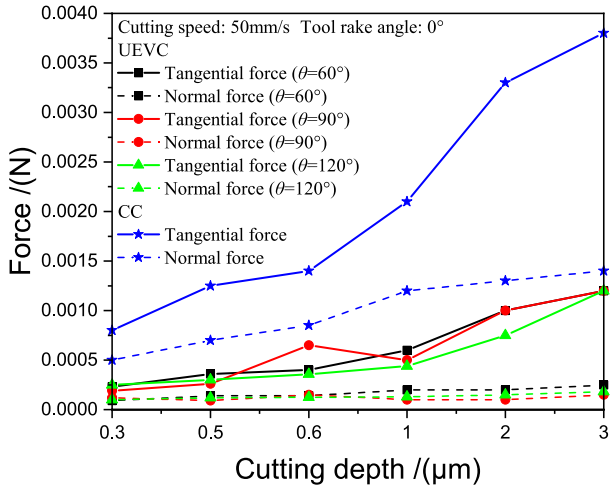

(a) Relationship of cutting depth and cutting force

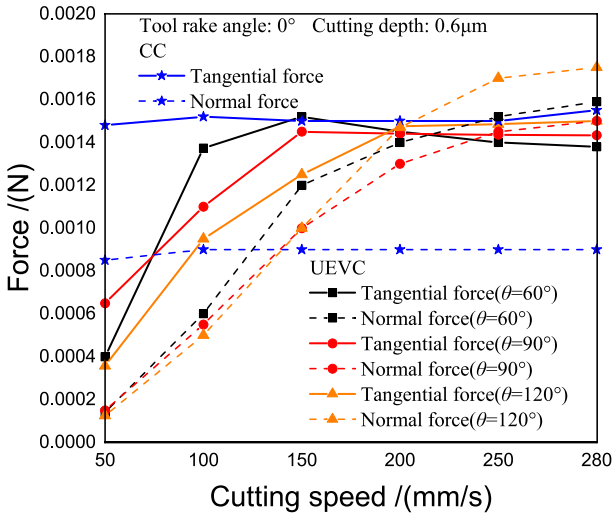

(b) Relationship of cutting speed and cutting force

Fig. 15 Comparison of cutting forces between UEVC and CC at different cutting depths and speeds

In Fig.15(b), the tangential cutting force of CC is always greater than the normal cutting force, and the cutting force first increases and then decreases slowly with the increase of cutting speed. This is because when the cutting speed is low, the tool tip will form built-up edge, then the cutting force will increase. When the cutting speed reaches a certain value, the built-up edge will disappear and the cutting force will be appropriately reduced (UEVC technology basically solves the problem of built-up edge due to the ultrasonic vibration). In UEVC machining, the tangential cutting force increases first and then decreases slowly with the increase of cutting speed, while the normal cutting force increases continuously. When the cutting speed is about 200 mm / s, the normal cutting force exceeds the tangential cutting force. This is because when the cutting speed exceeds the critical cutting speed, the elliptical cutting path of the tool tip changes from intermittent cutting to continuous cutting, and the contact time between the tool and the workpiece increases, making the normal cutting force become the dominant force. For the UEVC machining, the cutting speed is generally less than 1 / 2 of the critical speed. Therefore, the cutting force of UEVC is always lower than that of CC, and the cutting force with phase shift of 60° is lower than that of CC, which is more conducive to improve the surface quality.

Fig.16 shows the chip comparison between UEVC and CC under different cutting depths and speeds. With the increase of cutting depth, chip of UEVC is thinner and continuous than that of CC technology, which is more conducive to machining surface quality. When the cutting depth is less than 0.5 μm, although both UEVC and CC machining can both cause chip fracture, there are still some differences. The chip of CC machining is close to segment, while chip of UEVC continuity is better, which also proves that UEVC technology has the advantages of prolonging tool life and improving surface quality; with the increase of cutting speed, the chip thickness first increases and then decreases. In UEVC, the cutting speed has a great influence on the chip and the

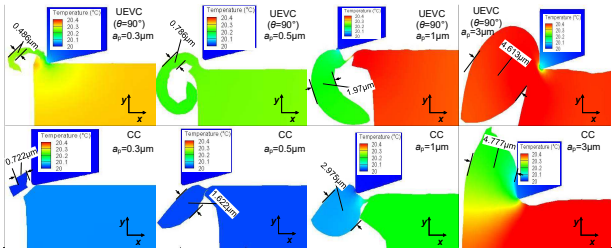

(a) Chips morphology of cutting depth

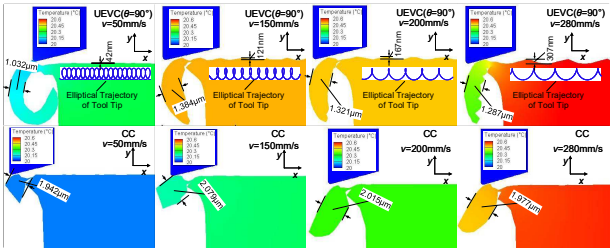

(b) Chips morphology of cutting speed

Fig. 16 Comparative analysis of chips between UEVC and CC at different cutting depths and speeds

residual height of the tool mark on the machined surface. For UEVC machining, the higher the cutting speed is, the smaller the overlapping area of the intermittent tool tip elliptic trajectory is until it exceeds the critical cutting speed and becomes continuous cutting. As a result, the maximum residual height increases, which leads to the decrease of machined surface quality and the enhancement of sawtooth on the back of chip. In CC machining, when the cutting speed is low, the sharpness of the tool decreases and the chip breaks. When the cutting speed is increased, the chip continuity becomes better, but too high cutting speed will also deteriorate the surface quality of machining.

Fig.17 shows the variation of chip thickness under different parameters of UEVC and CC. The trend of chip thickness is similar to that of cutting force, and the chip thickness of UEVC is much lower than that of CC. The larger the phase shift, the thinner the chip is. According to Fig.16(a) and Fig.17(a), it is found that when the cutting depth is less than 0.6 μm, the change of UEVC chip thickness is relatively stable, but it is easy to cause chip fracture; when the cutting depth is 0.6 μm to 2 μm, the increase rate of chip thickness is accelerated, and the chip continuity is good; when the cutting depth is greater than 2 μm, the chip thickness changes smoothly; when the cutting depth continues to increase, the chip thickness tends to the thickness of CC, and the advantage of UEVC is vanished. In Fig.17(b), the chip thickness first increases and then decreases. When the cutting speed is greater than 200 mm/s, the cutting thickness with phase shift of 120° exceeds that with the phase shift of 90°. This is because when the cutting speed is about 200 mm/s, the normal force with phase shift of 120° exceeds the

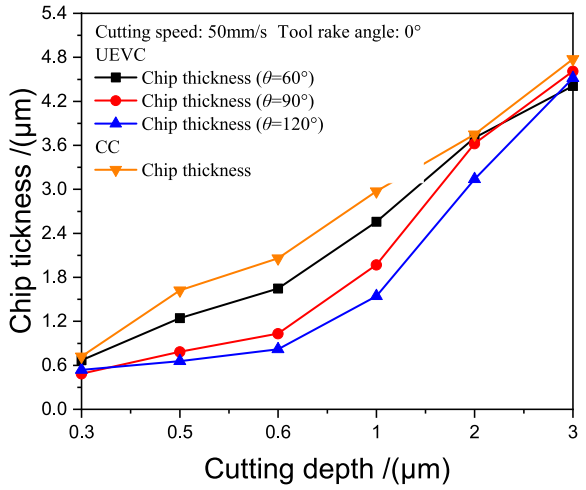

(a) Relationship between cutting depth and chip thickness

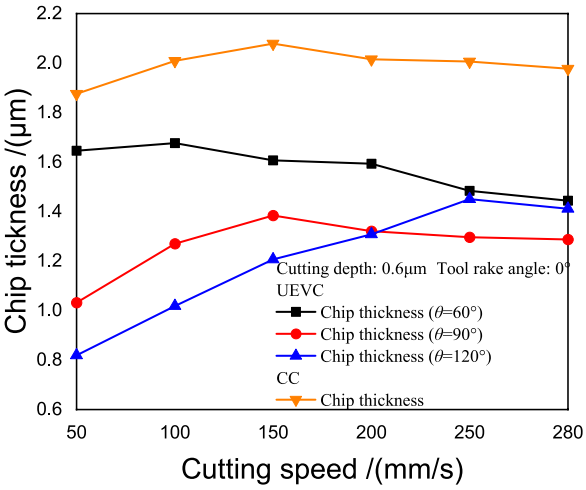

(b) Relationship between cutting speed and chip thickness

Fig. 17 Comparison of chip thickness between UEVC and CC at different cutting depths and speeds

main cutting force, which is conducive to chip removal.

5 Micro-pyramid Reflective Mold Cutting Based on The Guided Wave UEVC Technology

5.1 Experimental Facilities and Micro-pyramid Mold Machining Strategy

The micro-pyramid reflective is to imprint the micro-pyramid topological array on the surface of the film by the mold, so that the incident light passes through many times of reflection and refraction inside the film to form parallel reflected light, so as to realize the reflective function. As shown in Fig.18(a), the micro-pyramid array is obtained by three times of cutting in three directions with 60° intersection angle by using V-groove cutting method. Firstly, after finishing the

first cutting at a fixed interval, the mold is arranged in a V-shaped groove; secondly, the workpiece is rotated 60° for the second cutting to obtain the diamond surface; finally, the workpiece is rotated 120° to complete the third cutting to form a micro-pyramid array. To achieve high profile precision and mirror quality of micro-pyramid reflective mold, a five axis ultra-precision machine tool is used as the main facility of cutting experiment, and the cutting experimental research is carried out. The structure of the machine tool is shown in Fig.18(b). The X, Y and Z are linear axis driven by linear motor and fully constrained hydrostatic guide. The stroke of three linear axis is 350 mm, 300 mm and 150 mm; B-axis is the rotation axis, which is set on the Z-axis and is driven by brushless DC motor to achieve positioning accuracy of ± 1.0 arc seconds; C-axis is the spindle of machine tool with positioning function, which can achieve positioning accuracy of ± 1.0 arc seconds ; the coolant is oil mist. The guided wave UEVC device (resonance frequency 96.8 kHz and amplitude 0.55 μm) is fixed on the C-axis through an extension rod, and the workpiece is fixed on the B-axis rotation worktable. When the C-axis is fixed and the guided wave UEVC device has no excitation input, the cutting mode is conventional cutting. After inputting the excitation, it can be changed into ultrasonic elliptical vibration cutting. Through the translation of linear axis X, Y and Z axis and the rotation of B-axis, the micro-pyramid topological array is realized.

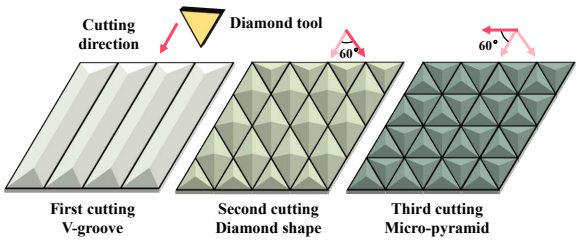

(a) Micro-pyramid reflective mold machining strategy

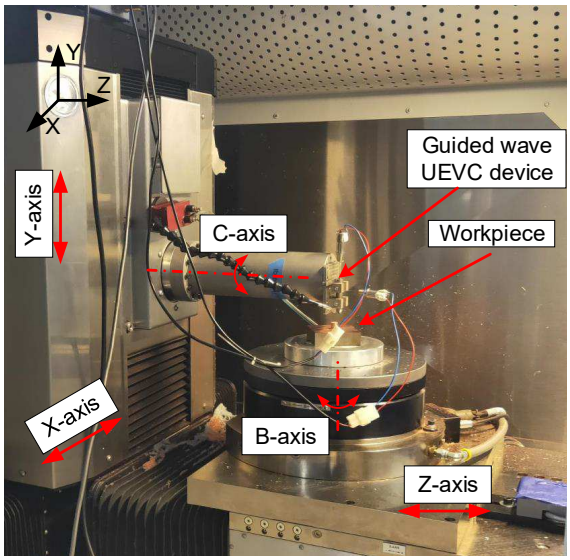

(b) Five-axis machine tool with guided wave UEVC device

Fig. 18 Five-axis ultra-precision machine tool and micro-pyramid reflective mold machining strategy

5.2 Comparative Experiment of Plane Machining With UEVC and CC

Fig.19 shows the plane cutting experiments of UEVC and CC at different cutting depths. When using UEVC technology, the cutting depth below 3 μm has little influence on surface roughness, and the surface roughness is better at cutting depth 0.6 μm which is 0.014 μm. In CC processing, the varied cutting depths lead to the varying degree of tool mark and residue on machined surface, and the better roughness is 0.032 μm when the cutting depth is 1.2 μm. According to Fig.19(b), the surface roughness obtained by UEVC at the same cutting depth is superior to CC. Tiny cutting depth results in crumpled chip, while excessive cutting depth increases the cutting resistance, both of which tend to deteriorate the machined surface.

Fig.20 shows the Comparison of UEVC and CC plane machining under varied cutting speeds. With the increase of cutting speed, the residual height of tool marks in the cutting direction of UEVC machining significant increase, especially when the cutting speed exceeds the critical cutting speed. In CC machining, both sides of Z direction (feed direction) are extruded each other, and there are large sticky substances on the surface. In comparison, the UEVC technology restrains the extrusion and tool marks through plane machining, and the surface quality is better than that of CC. Fig.20(b) shows the roughness of CC and UEVC, the surface roughness of UEVC machining is the minimum at 0.015 μm when the cutting speed is 50 mm/s. When the cutting speed exceeds the critical cutting speed ($\geq$ 280 mm/s), the surface roughness growth obviously, while the surface roughness of CC machining is the minimum at 0.043 μm when the cutting speed of 125 mm/s. Compared with CC, the surface roughness of UEVC is smaller and the surface roughness is reduced by 50%.

The chips of plane cutting are collected at the cutting speed is 125 mm/s, the cutting depth is 1.2 μm, and the feed rate is 0.5 μm. The SEM results are shown in Figure 21. The chip in CC is thicker, continuous and banded, while the chip in UEVC is thinner and the curl curvature is larger, which is conducive to chip removal. It can be seen that the chip accumulation obtained by UEVC is denser, which shows that UEVC can effectively suppress the generation of the saw-tooth chip and maintain cutting process stability.

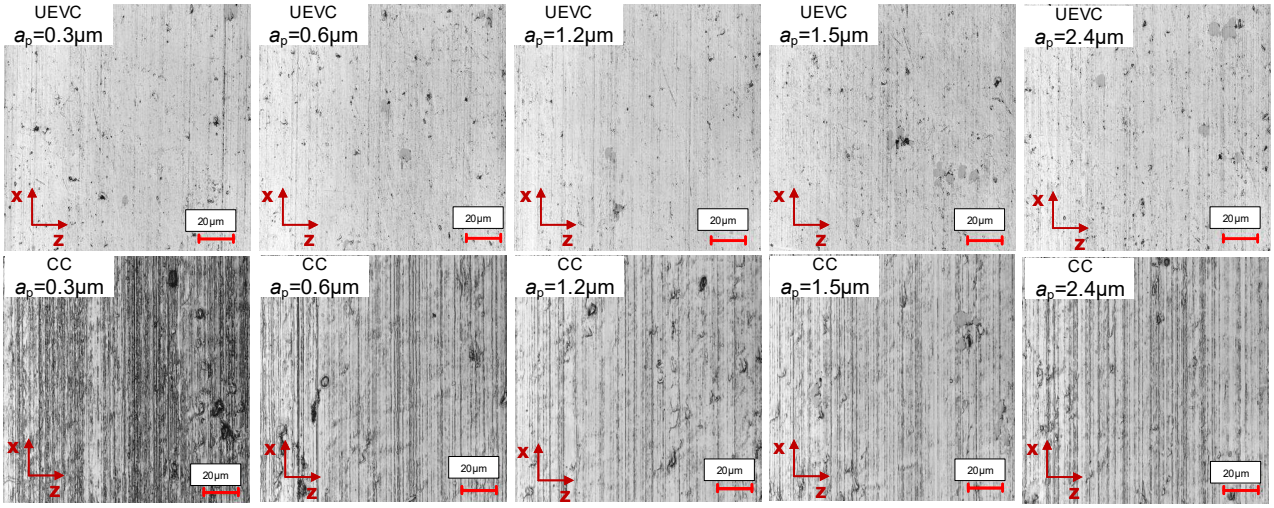

(a) Surface morphology of UEVC and CC plane machining

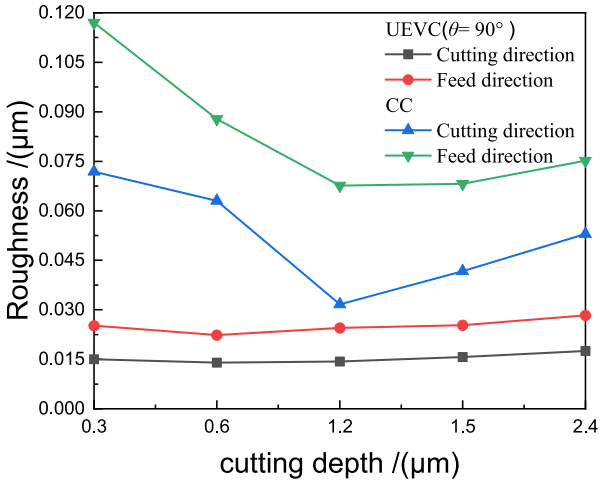

(b) Surface roughness of UEVC and CC plane machining

Fig. 19 Comparison of UEVC and CC plane machining under varied cutting depths

5.3 Experiments of The Micro-pyramid Reflective Mold in Guided Wave UEVC

Fig.22(a) is the SEM test of the micro-pyramid reflective mold in UEVC and CC. It can be found that there are some chips remain in the V-groove during CC processing, while the chips residual doesn't exist in UEVC processing. Moreover, the UEVC processing takes the advantages of suppressing the burr, especially in the intersection of the three cutting directions at the bottom of the micro-pyramid. UEVC only produces small material extrusion in local area but does not form burr. In UEVC machining, compared with the oxygen free copper mold, the surface of single crystal copper mold forms many "wrinkles", which is due to the friction between the tool and the workpiece surface due to other material characteristics, resulting in the regenerative chatter of the cutting system. Fig.22(b) and 22(c) show the results of micro-pyramid reflective mold and surface roughness measurement. The processing angle of V-groove is 70.57° and the average roughness of three surfaces of one single micro-pyramid element is 5.21 nm, the maximum roughness is 8.02 nm, and the minimum roughness is 3.84 nm. Through this experiment, the applicability of guided wave UEVC in the manufacturing of micro-pyramid mold is verified, and the micro-pyramid mold with mirror quality is obtained.

6 Discussions and Conclusions

In order to achieve high profile precision and mirror quality of micro-pyramid reflective mold, this paper introduces the guided wave UEVC device by combining the ultrasonic elliptical vibration cutting with guided wave transmission technology. The mechanism of orthogonal coupling of transverse and longitudinal guided wave bands in orthogonal UEVC

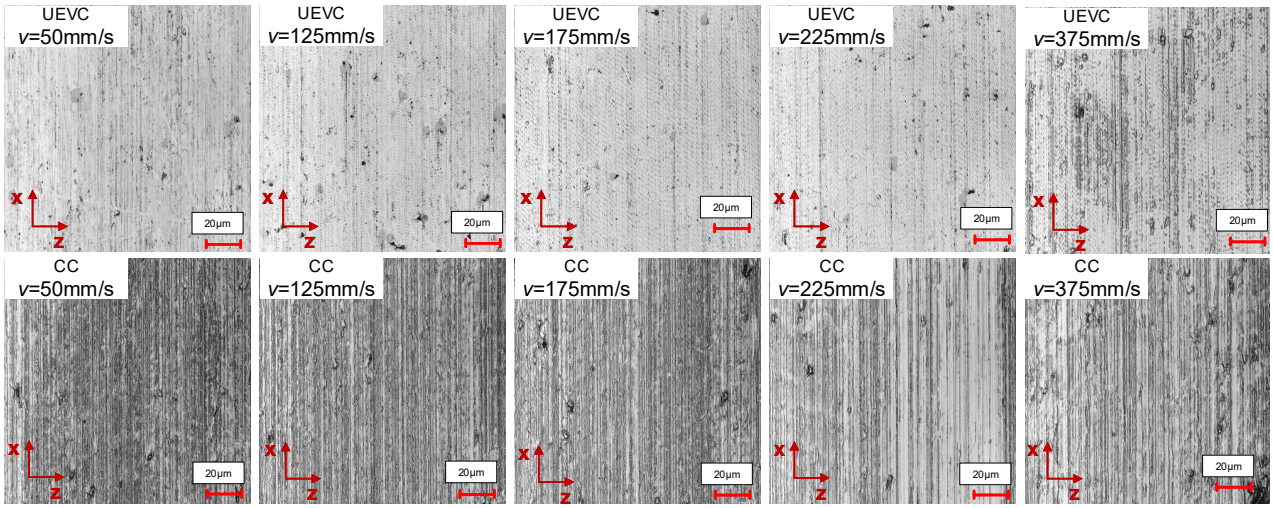

(a) Surface morphology of UEVC and CC

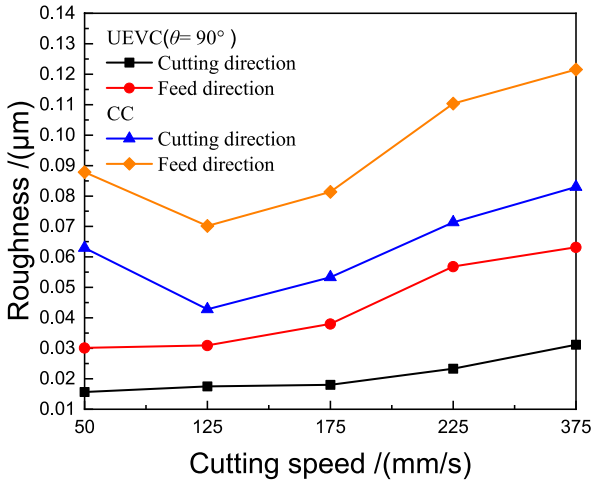

(b) Surface roughness of UEVC and CC

Fig. 20 Comparison of UEVC and CC plane machining under varied cutting speed

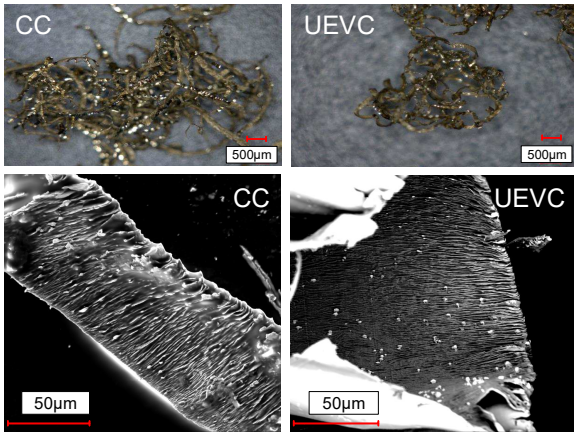

Fig. 21 The elliptic trajectory of the guided wave UEVC device

device is analyzed by using dynamic principle, and the influence of bending guided wave band on longitudinal vibration is expounded. The control model of tool tip elliptic trajectory deflection is established, and the influence of ellipse deflection angle on amplitude and phase shift is analyzed. FEA is used to carry out the change of cutting force and chip under variable deflection angle of the elliptic trajectory. Finally, the applicability of high-frequency guided wave UEVC in ultra-precision machining is verified, and the high-precision and mirror quality machining of micro-pyramid reflective mold is completed by carrying out the comparison experiment of the UEVC and CC plane machining and micro-pyramid machining. The main conclusions are as follows:

1.In order to avoid the influence of bending vibration on the longitudinal vibration, the plate-type guided wave band should be chosen a smaller diameter and thickness, then dual longitudinal vibration transducers can transmit longitudinal vibration independently through the guided wave band and obtain better coupling effect. Based on this theory, the or-

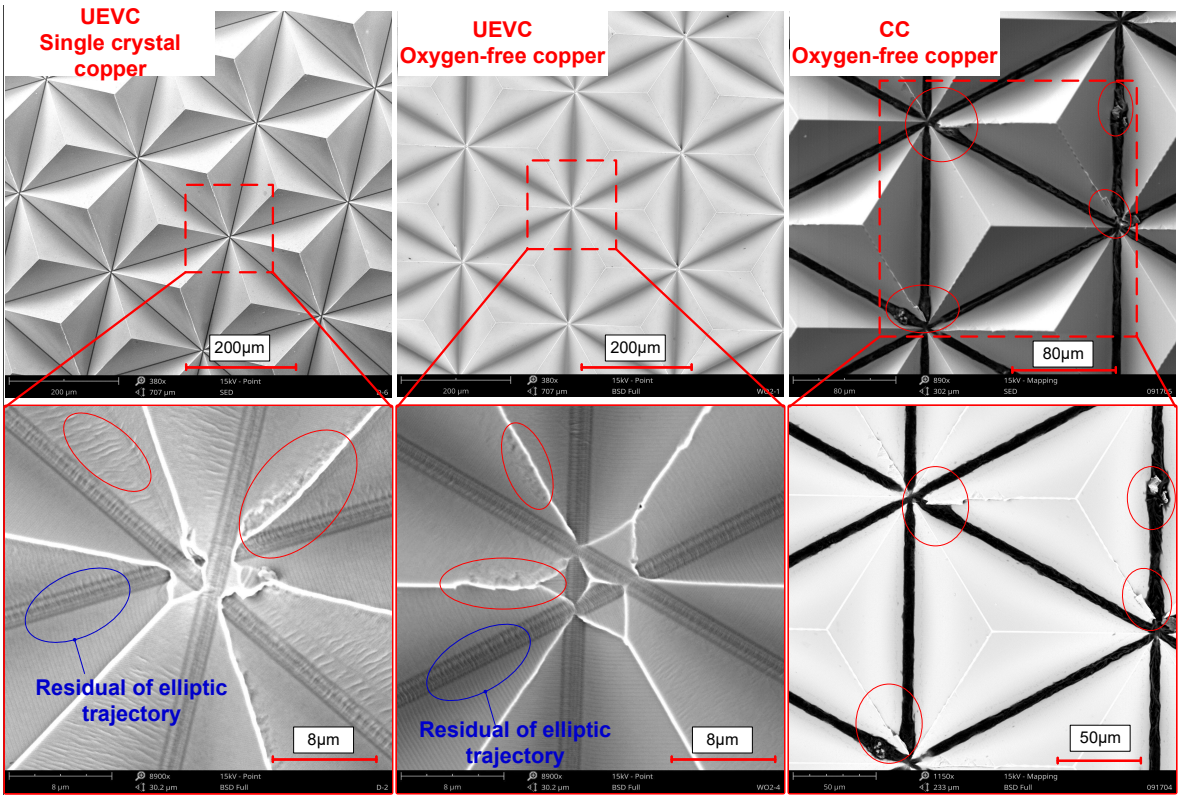

(a) SEM test of the micro-pyramid array machined in guided wave UEVC and CC

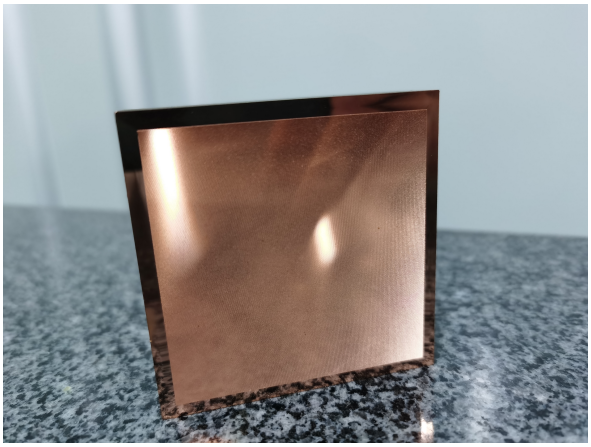

(b) Micro-pyramid reflective mold with guided wave UEVC

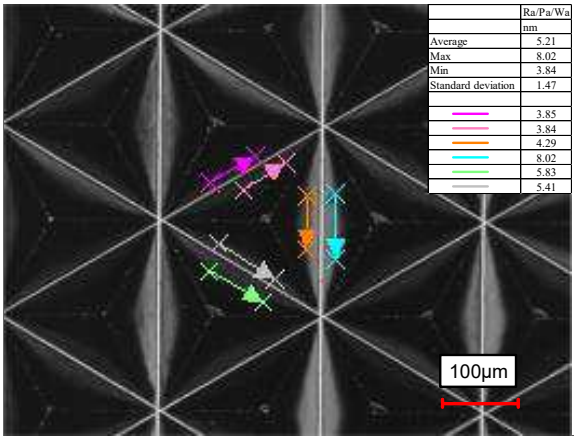

(c) Surface roughness of the micro-pyramid element

Fig. 22 The cutting experiment of the micro-pyramid reflective mold in guided wave UEVC and CC

thogonal guided wave UEVC device is fabricated with resonance frequency of 96.8 kHz and orthogonal amplitude of 0.55 μm and 0.46 μm, respectively. At the same time, the uniformity between the actual elliptic trajectory generated by the device and the ideal elliptic trajectory is good, which shows that the device has high precision and easy to control.
2.The FEA results show that when the tool tip elliptic trajectory changes from VET to HET (amplitude $n > m$), the cutting force is small and stable when the deflection angle η is between 10° and 70°, the lowest is at about 20° and 70°. At the same time, the chip curl curvature of HET (η = 90°) is smaller, which indicates that the tool has lower sharpness and less impact, and is suitable for brittle materials processing; VET (η = 0°) chip turns into spiral curl curvature, which indicates that the cutter has higher sharpness and is suitable for processing high hardness materials. Compared with CC, UEVC can obtain better surface quality when cutting depth is 0.3 μm-0.6 μm and cutting speed is 50 mm/s-100 mm/s.
3.The results of plane cutting experiments show that the op-

timal cutting parameters of UEVC (cutting depth 0.6 μm, cutting speed of 50 mm/s) are obtained; compared with CC machining, UEVC can get more dense chip, which indicates that the chip accumulation obtained by UEVC is denser. Finally, the micro pyramid reflective mold with an average roughness of 5.21 nm can be obtained by using the guided wave UEVC device.

Acknowledgements

This research was funded by Natural Science Foundation of Fujian Province (No.2019J01327), Educational Research Projects of Young and Middle-Aged Teachers of Fujian Province (No.JAT200251) and National Natural Science Foundation Cultivation Program of Jimei University (No.ZP2020048). The authors would also like to thank Mr. Yu'an Jiang for his contribution to the disposal data and experiment advice.

Ethical Approval

This material is the authors' own original work, which has not been previously published elsewhere.

Consent to Participate

Not applicable

Consent to Publish

The authors have read and agreed to the published version of the manuscript.

Authous Contributions

Tao Jiang: methodology, formal analysis, writing-original draft. Jintao Yang: data curation, validation. Jun Pi: conceptualization, funding acquisiton. Wenyu Luo: visualization, software. Jun Zhang: writing-review and editing, resources.

Funding

This research was funded by Natural Science Foundation of Fujian Province (No.2019J01327), Educational Research Projects of Young and Middle-Aged Teachers of Fujian Province (No.JAT200251) and National Natural Science Foundation Cultivation Program of Jimei University (No.ZP2020048).

Conflict of Interest

The authors declare that they have no conflict of interest.

Avaliability of data and materials

Not applicable

References

1. Fashina A, Adama K, Oyewole O, Anye V, Asare J, Zebaze Kana M, Soboyejo W (2015) Surface texture and optical properties of crystalline silicon substrates. Journal of Renewable and Sustainable Energy 7(6):063119, https://doi.org/10.1063/1.4937117
2. Wang ZW, Chen MW, Wu JW, Zheng HH, Zheng XF (2010) A review of surface texture of tribological interfaces. In: Advances in Engineering Design and Optimization, Trans Tech Publ, Applied Mechanics and Materials, vol 37, pp 41–45, https://doi.org/10.4028/www.scientific.net/AMM.37-38.41
3. Dana KJ, Van Ginneken B, Nayar SK, Koenderink JJ (1999) Reflectance and texture of real-world surfaces. ACM Transactions On Graphics (TOG) 18(1):1–34, https://doi.org/10.1145/300776.300778
4. Wang J, Liao WH, Guo P (2020) Modulated ultrasonic elliptical vibration cutting for ductile-regime texturing of brittle materials with 2-d combined resonant and non-resonant vibrations. International Journal of Mechanical Sciences 170:105347, https://doi.org/10.1016/j.ijmecsci.2019.105347
5. Arslan A, Masjuki H, Kalam M, Varman M, Mufti R, Mosarof M, Khuong L, Quazi M (2016) Surface texture manufacturing techniques and tribological effect of surface texturing on cutting tool performance: a review. Critical Reviews in Solid State and Materials Sciences 41(6):447–481, https://doi.org/10.1080/10408436.2016.1186597
6. De Felicis D, Mughal MZ, Bemporad E (2017) A method to improve the quality of 2.5 dimensional micro-and nano-structures produced by focused ion beam machining. Micron 101:8–15, https://doi.org/10.1016/j.micron.2017.05.005
7. Shamoto E, Moriwaki T (1994) Study on elliptical vibration cutting. CIRP annals 43(1):35–38, https://doi.org/10.1016/S0007-8506(07)62158-1
8. Moriwaki T, Shamoto E (1995) Ultrasonic elliptical vibration cutting. CIRP annals 44(1):31–34, https://doi.org/10.1016/S0007-8506(07)62269-0
9. Shamoto E, Moriwaki T (1999) Ultaprecision diamond cutting of hardened steel by applying ellip-

tical vibration cutting. CIRP Annals 48(1):441–444, https://doi.org/10.1016/S0007-8506(07)63222-3
10. Suzuki N, Haritani M, Yang Jb, Hino R, Shamoto E (2007) Elliptical vibration cutting of tungsten alloy molds for optical glass parts. CIRP annals 56(1):127–130, https://doi.org/10.1016/j.cirp.2007.05.032
11. Kim GD, Loh BG (2010) Machining of micro-channels and pyramid patterns using elliptical vibration cutting. The International Journal of Advanced Manufacturing Technology 49(9):961–968, https://doi.org/10.1007/s00170-009-2451-7
12. Guo P, Ehmann KF (2013) Development of a tertiary motion generator for elliptical vibration texturing. Precision Engineering 37(2):364–371, https://doi.org/10.1016/j.precisioneng.2012.10.005
13. Ma C, Shamoto E, Moriwaki T, Wang L (2004) Study of machining accuracy in ultrasonic elliptical vibration cutting. International Journal of Machine Tools and Manufacture 44(12-13):1305–1310, https://doi.org/10.1016/j.ijmachtools.2004.04.014
14. Nath C, Zhang X, Senthil A, Rahman M (2014) 11.17 - ultrasonic vibration cutting: Part ii: Ductile cutting and analytical force models for the elliptical vibration cutting process. In: Hashmi S, Batalha GF, Van Tyne CJ, Yilbas B (eds) Comprehensive Materials Processing, Elsevier, Oxford, pp 455–481, https://doi.org/10.1016/B978-0-08-096532-1.01328-5
15. Zhou M, Eow Y, Ngoi B, Lim E (2003) Vibration-assisted precision machining of steel with pcd tools. Materials and manufacturing processes 18(5):825–834, https://doi.org/10.1081/AMP-120024978
16. Saito H, Jung H, Shamoto E (2016) Elliptical vibration cutting of hardened die steel with coated carbide tools. Precision Engineering 45:44–54, https://doi.org/10.1016/j.precisioneng.2016.01.004
17. Zhang X, Kumar AS, Rahman M, Nath C, Liu K (2011) Experimental study on ultrasonic elliptical vibration cutting of hardened steel using pcd tools. Journal of Materials Processing Technology 211(11):1701–1709, https://doi.org/10.1016/j.jmatprotec.2011.05.015
18. Zhang X, Kumar AS, Rahman M, Nath C, Liu K (2012) An analytical force model for orthogonal elliptical vibration cutting technique. Journal of manufacturing processes 14(3):378–387, https://doi.org/10.1016/j.jmapro.2012.05.006
19. Jiang X, Zhang X, Zhu X, Sui H, Zhang D (2017) Study of phase shift control in high-speed ultrasonic vibration cutting. IEEE Transactions on Industrial Electronics 65(3):2467–2474, https://doi.org/10.1109/TIE.2017.2740827
20. Kim GD, Loh BG (2007) Characteristics of elliptical vibration cutting in micro-v grooving with variations in the elliptical cutting locus and excitation frequency. Journal of micromechanics and microengineering 18(2):025002, https://doi.org/10.1088/0960-1317/18/2/025002
21. Kim GD, Loh BG (2007) Characteristics of chip formation in micro v-grooving using elliptical vibration cutting. Journal of micromechanics and microengineering 17(8):1458, https://doi.org/10.1088/0960-1317/17/8/007
22. Kim GD, Loh BG (2011) Direct machining of micro patterns on nickel alloy and mold steel by vibration assisted cutting. International journal of precision engineering and manufacturing 12(4):583–588, https://doi.org/10.1007/s12541-011-0075-y
23. Lin J, Guan L, Lu M, Han J, Kan Y (2017) Modeling and analysis of the chip formation and transient cutting force during elliptical vibration cutting process. AIP Advances 7(12):125101, https://doi.org/10.1063/1.5006303
24. Zhang X, Kumar AS, Rahman M (2012) Effects of cutting and vibration parameters on transient cutting force in elliptical vibration cutting. In: International Conference on Intelligent Robotics, Automation, and Manufacturing, Springer, pp 483–490, https://doi.org/10.1007/978-3-642-35197-6_54
25. Jieqiong L, Jinguo H, Xiaoqin Z, Zhaopeng H, Mingming L (2016) Study on predictive model of cutting force and geometry parameters for oblique elliptical vibration cutting. International Journal of Mechanical Sciences 117:43–52, https://doi.org/10.1016/j.ijmecsci.2016.08.004
26. Suzuki N, Yokoi H, Shamoto E (2011) Micro/nano sculpturing of hardened steel by controlling vibration amplitude in elliptical vibration cutting. Precision Engineering 35(1):44–50, https://doi.org/10.1016/j.precisioneng.2010.09.006
27. Zhang J, Suzuki N, Wang Y, Shamoto E (2017) Influence of clearance angle on micro/nano structure fabrication in elliptical vibration cutting of hardened steel. International Journal of Nanomanufacturing 13(4):351–361, https://doi.org/10.1504/IJNM.2017.087536
28. Kim GD, Loh BG (2013) Cutting force variation with respect to tilt angle of trajectory in elliptical vibration v-grooving. International journal of precision engineering and manufacturing 14(10):1861–1864, 10.1007/s12541-013-0249-x
29. Jiang Y, Pi J, Zhang Y, Jiang T, Yang G, Shen Z (2020) Research on the tool tip trajectory deflection control and cutting characteristics of elliptical vibration cutting based on guided wave transmission. The International Journal of Advanced Manufacturing Technology 108(9):3101–3117, https://doi.org/10.1007/s00170-020-05552-y

Figures

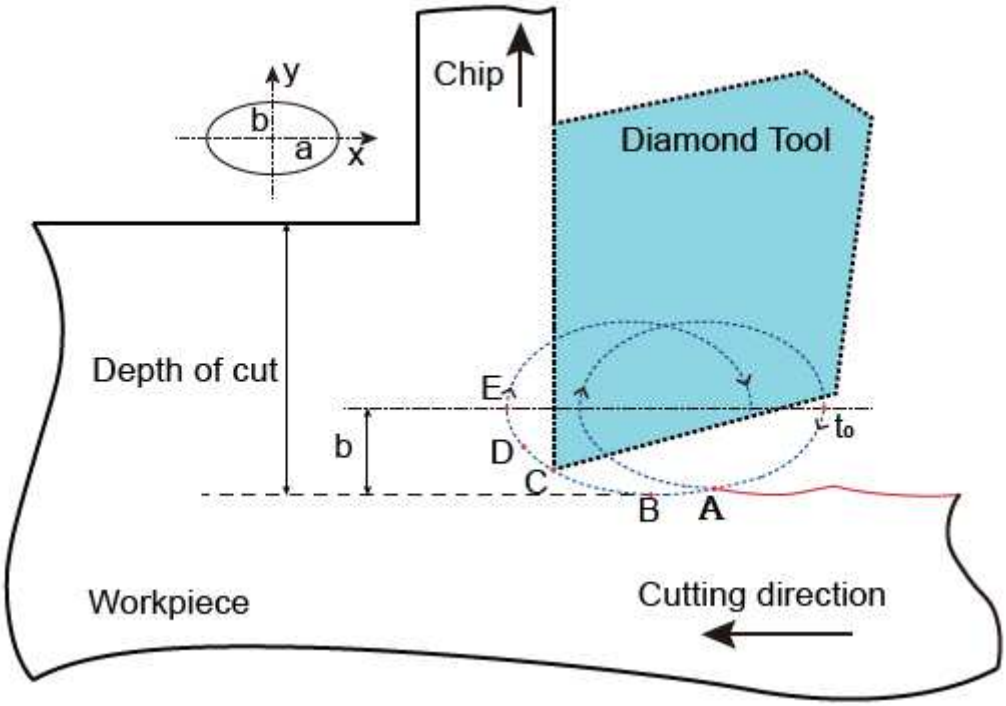

Figure 1

Elliptical vibration cutting process

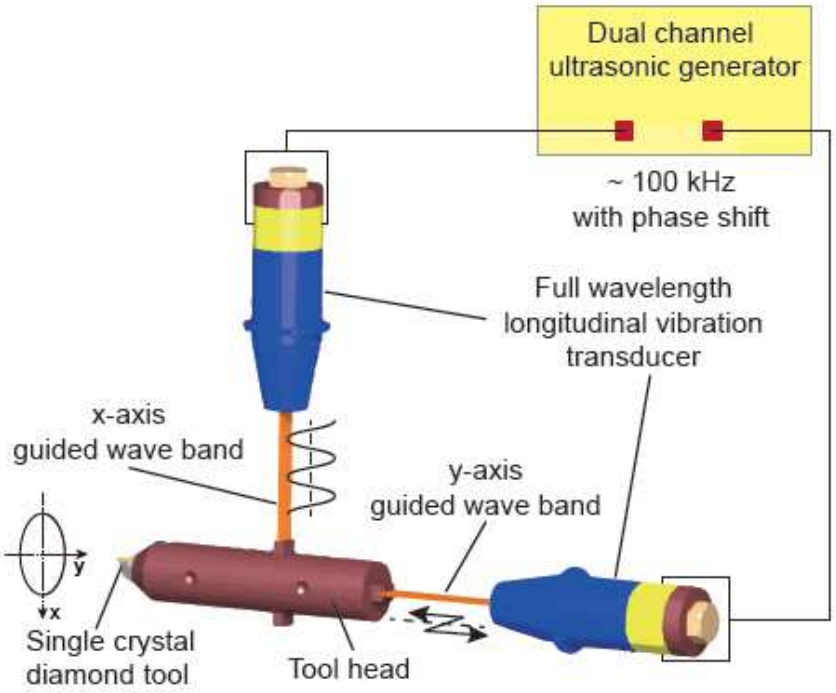

(a) Schematic diagram of the orthogonal guided wave UEVC device

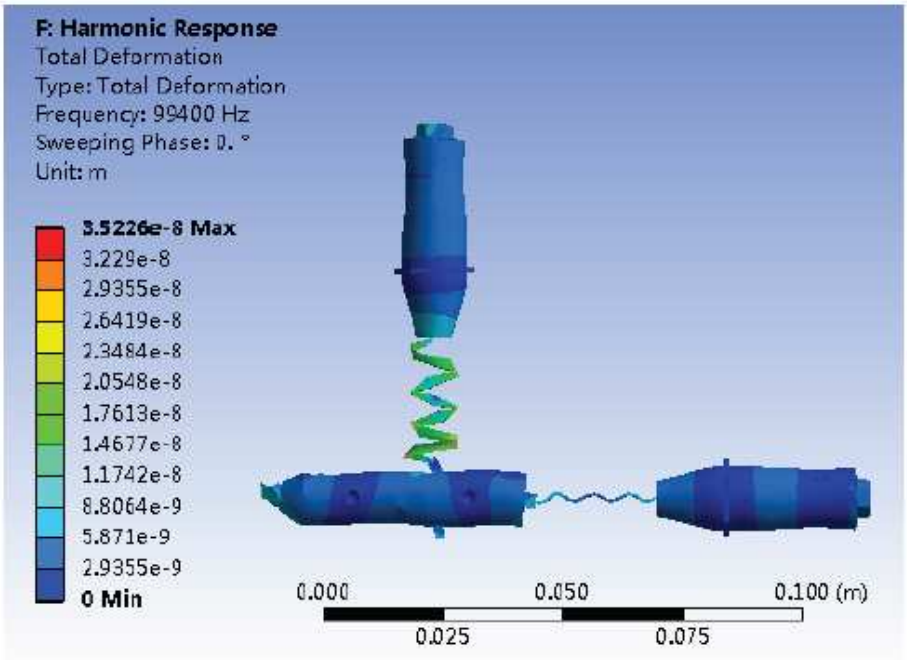

(b) Harmonic response simulation of the guided wave UEVC device

Figure 2

Guided wave UEVC device

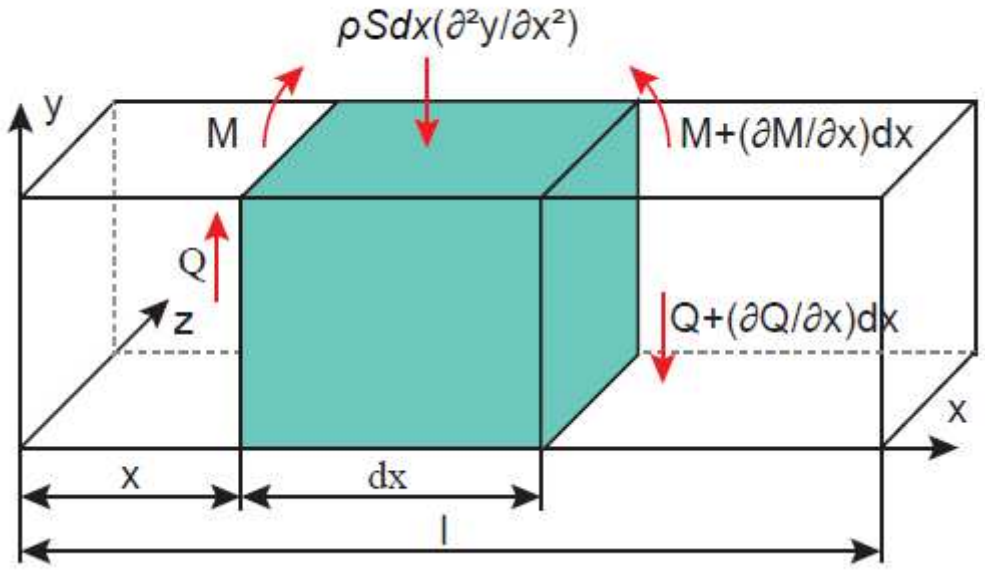

Figure 3

Transverse free vibration model of guided wave band

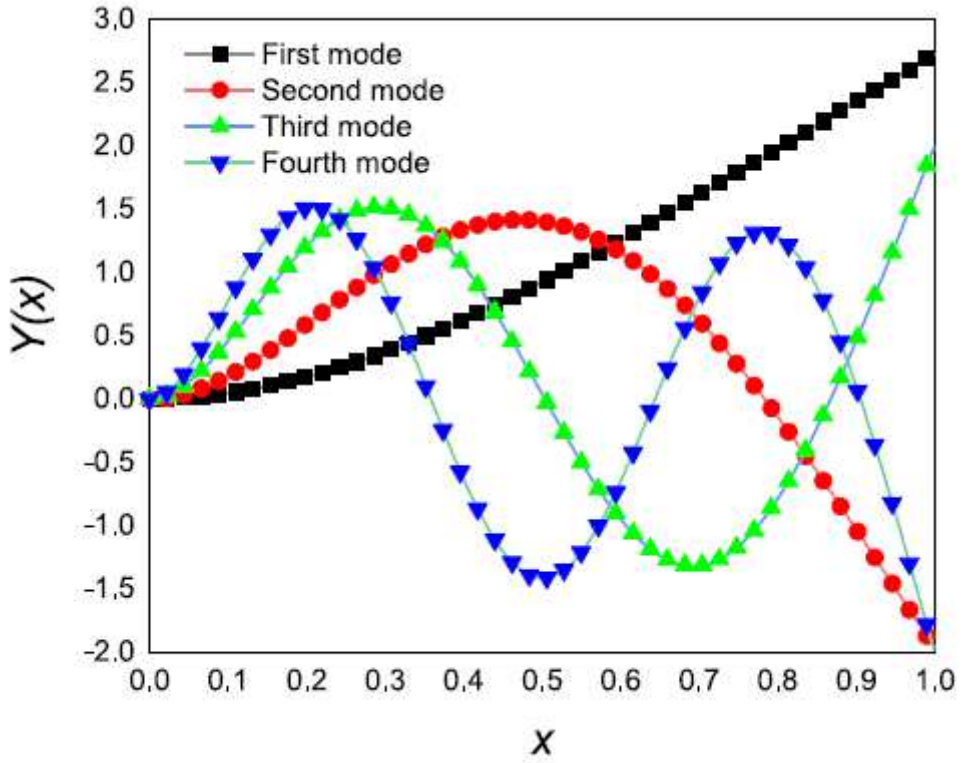

Figure 4

Bending mode of guided wave band in orthogonal UEVC device

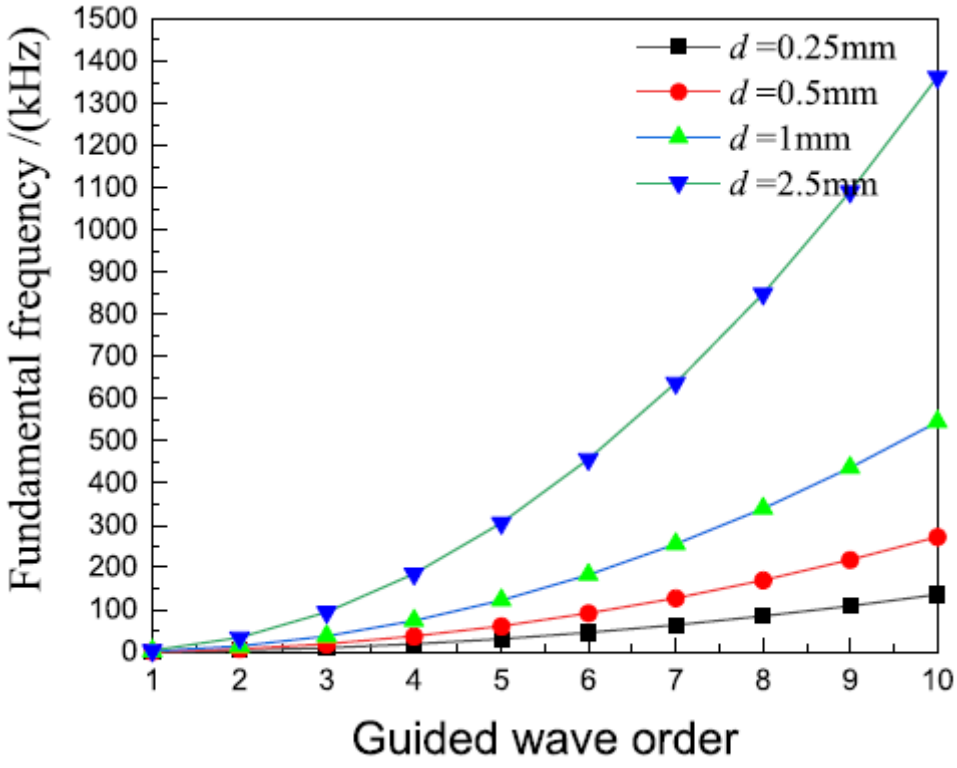

Figure 5

The relation between the order of the plate-shaped guided wave band and the fundamental frequency of bending vibration

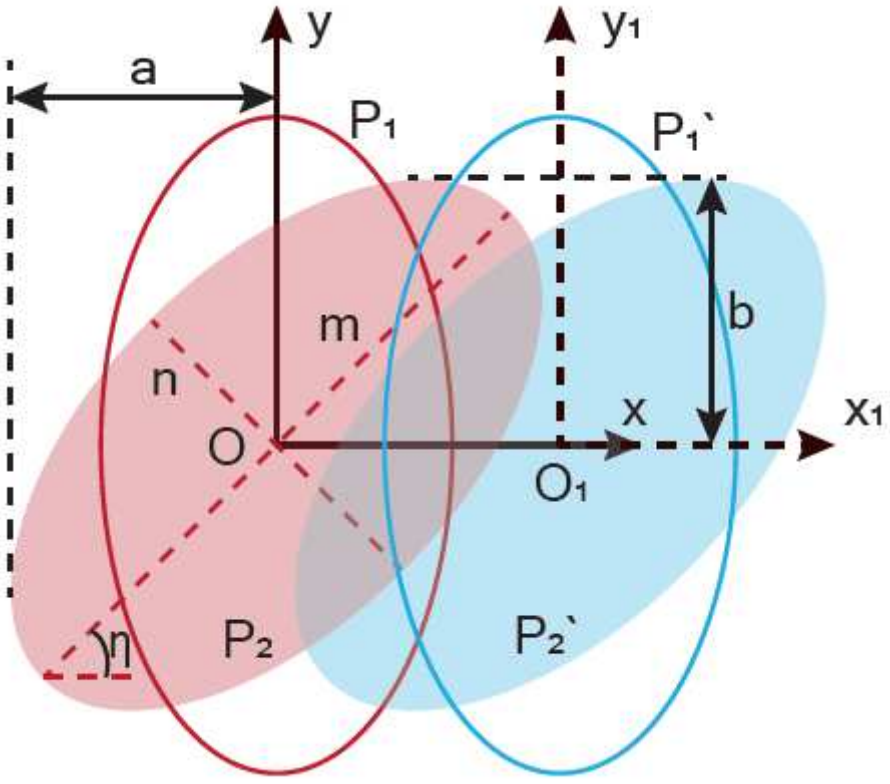

Figure 6

Tool tip elliptic trajectory deflection model

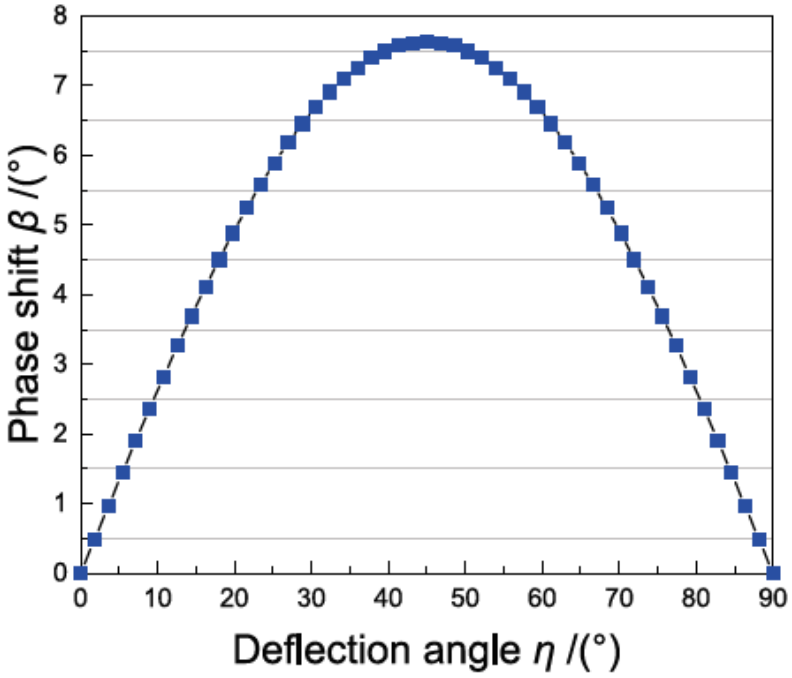

(a) The relationship between deflection angle and phase shift after deflection

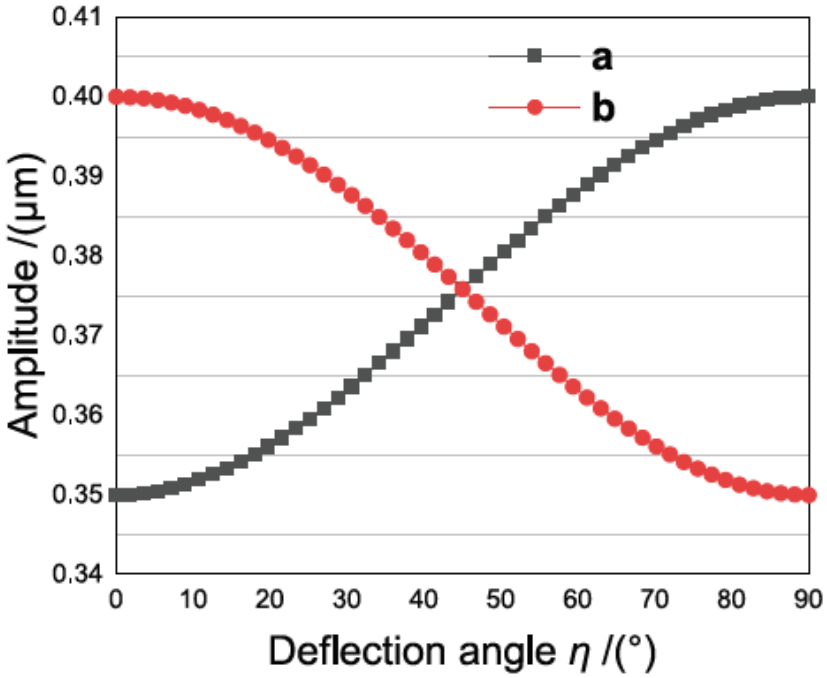

(b) The relationship between deflection angle and amplitude after deflection

Figure 7

The relationships between deflection angle and phase shift and amplitude

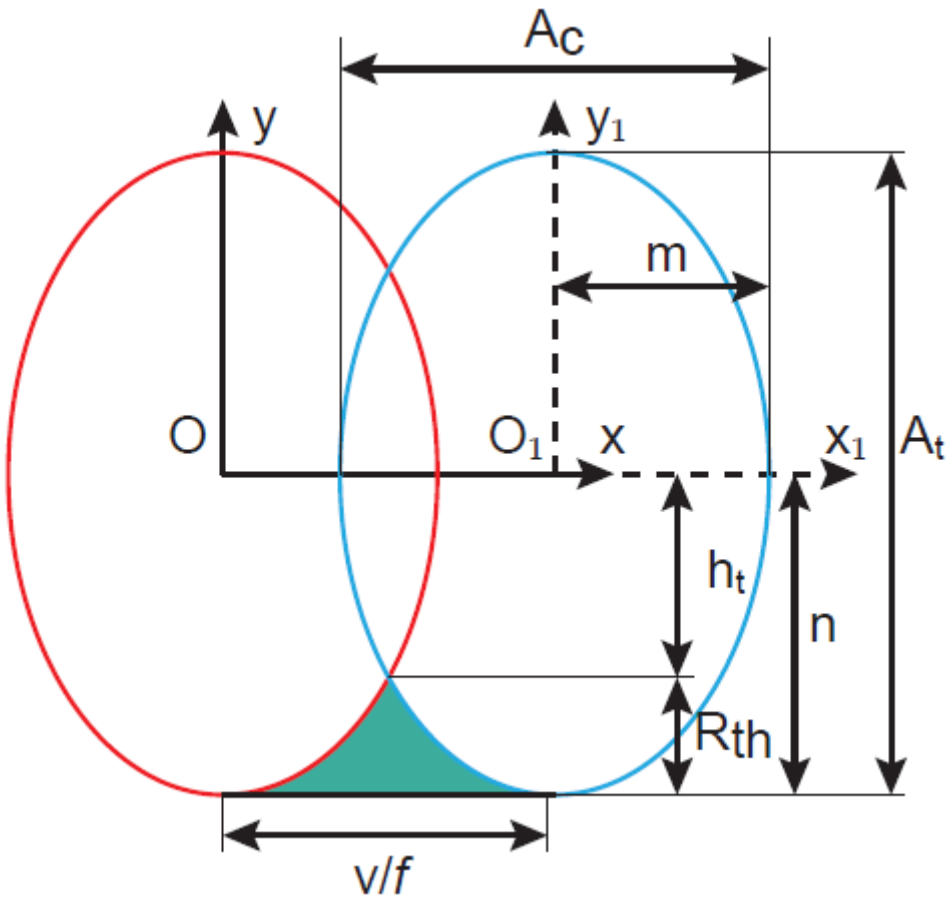

Figure 8

Model of the residual height of elliptic trajectory

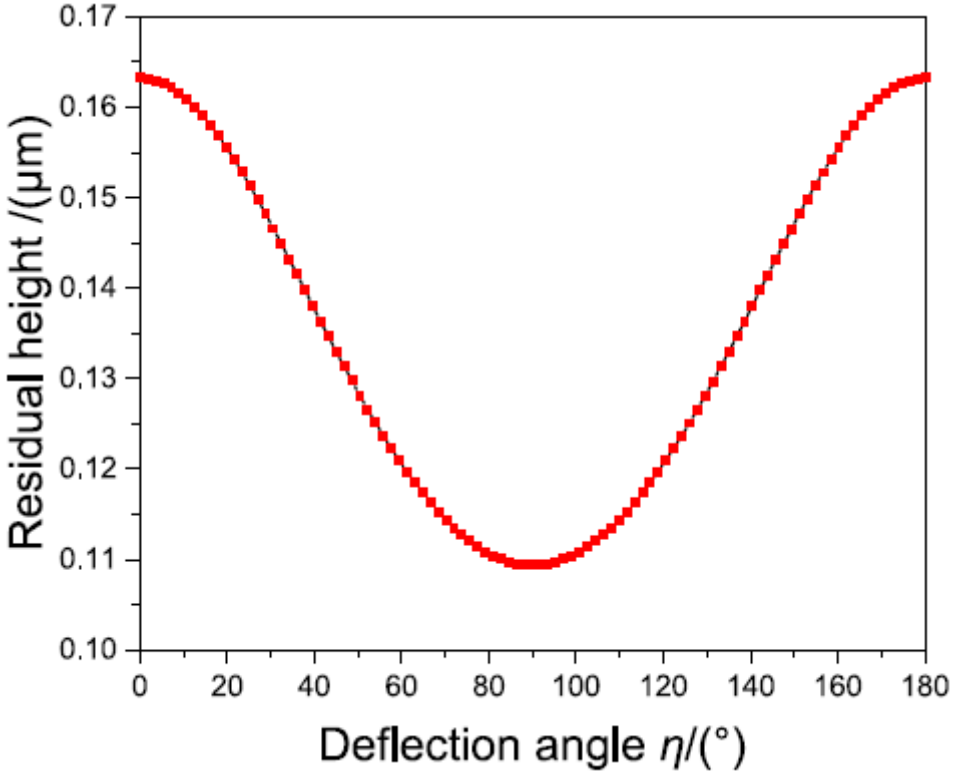

Figure 9

Relationship between the residual height and the deflection angle of elliptic trajectory

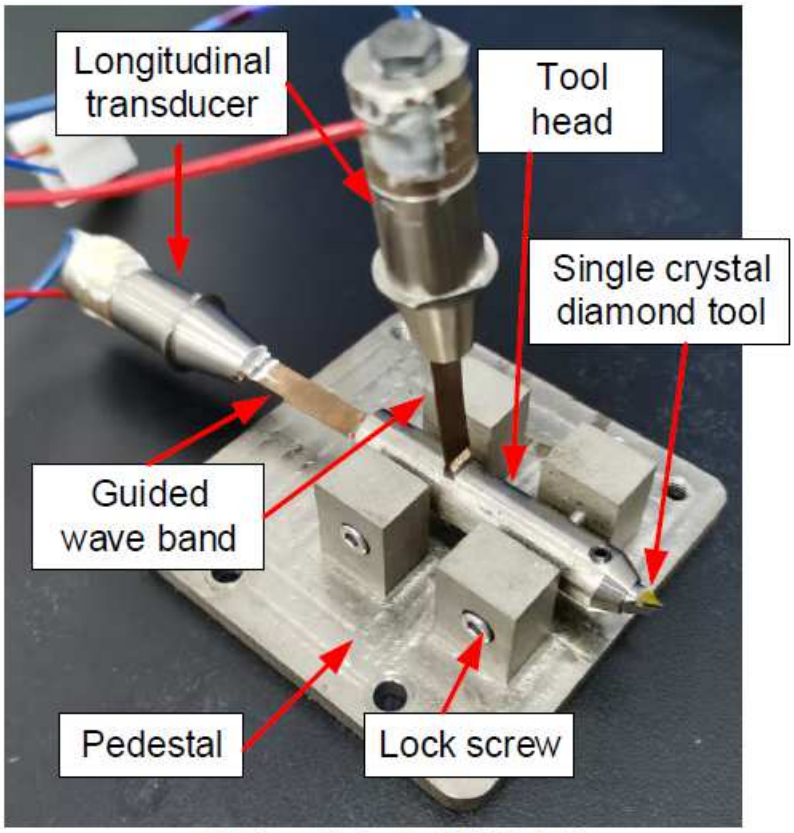

(a) The guided wave UEVC device

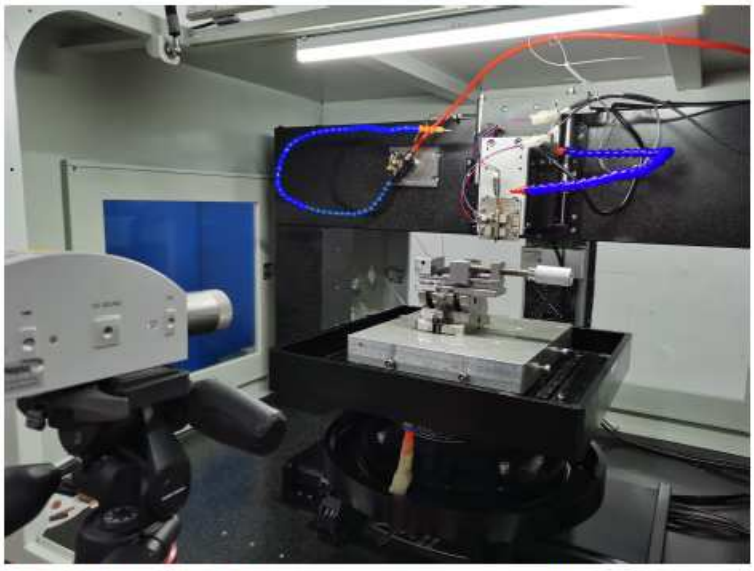

(b) Test of resonant frequency and amplitude with laser vibrometer

Figure 10

The guided wave UEVC device and the test of resonant frequency and amplitude

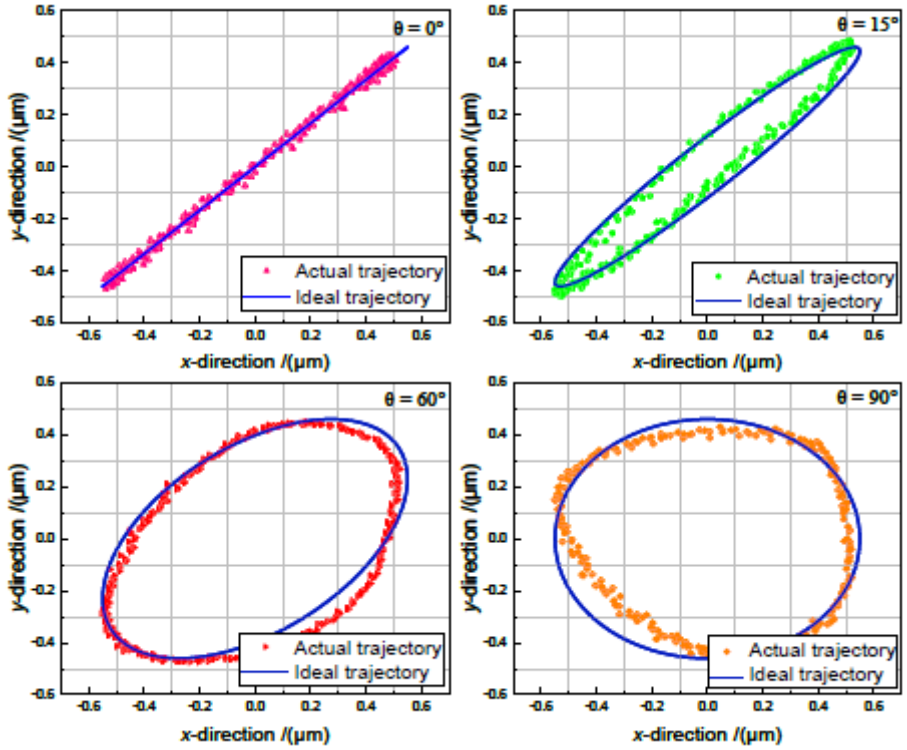

Figure 11

The elliptic trajectory of the guided wave UEVC device

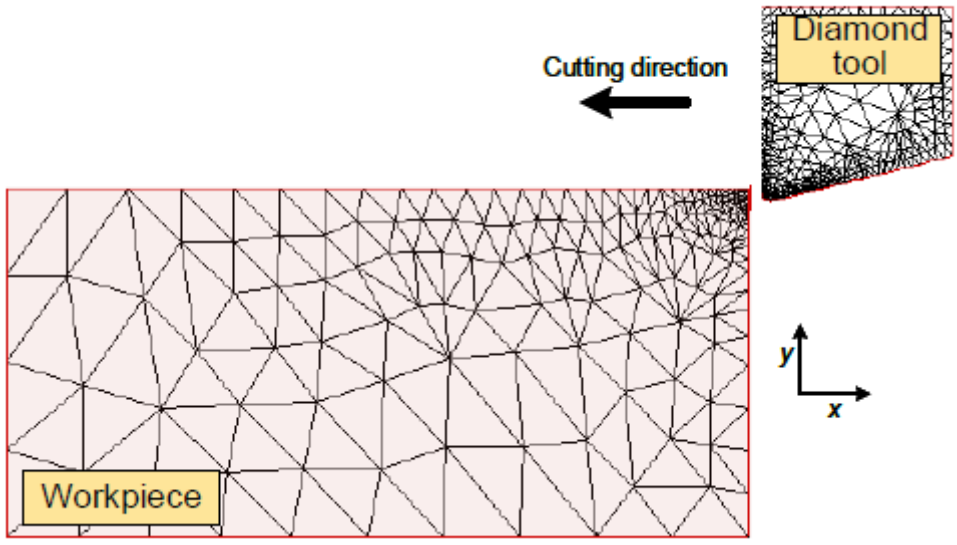

Figure 12

FEA model of the UEVC

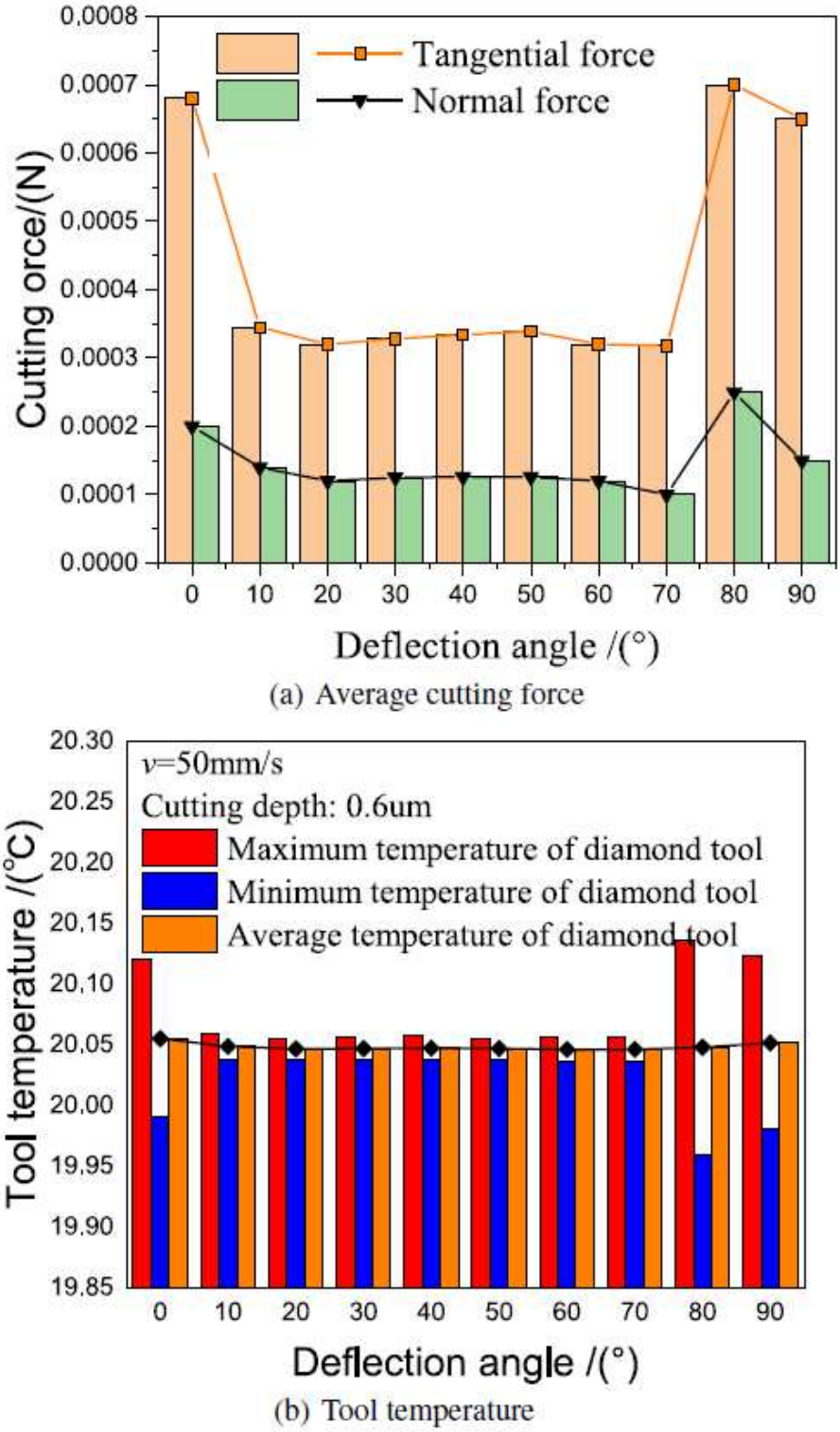

Figure 13

Simulation of the cutting force and temperature of the tool in UEVC with variable deflection angle

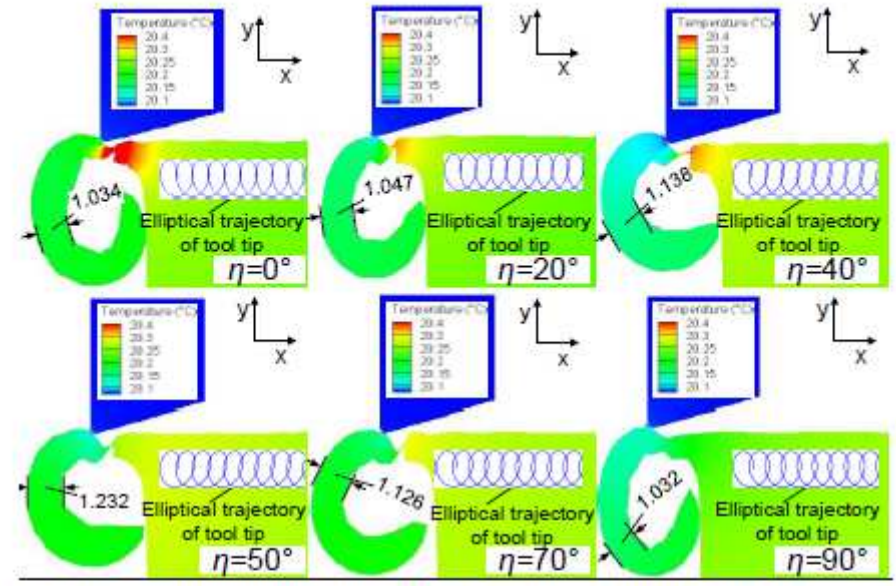

(a) The morphology of the UEVC with varied deflection angle

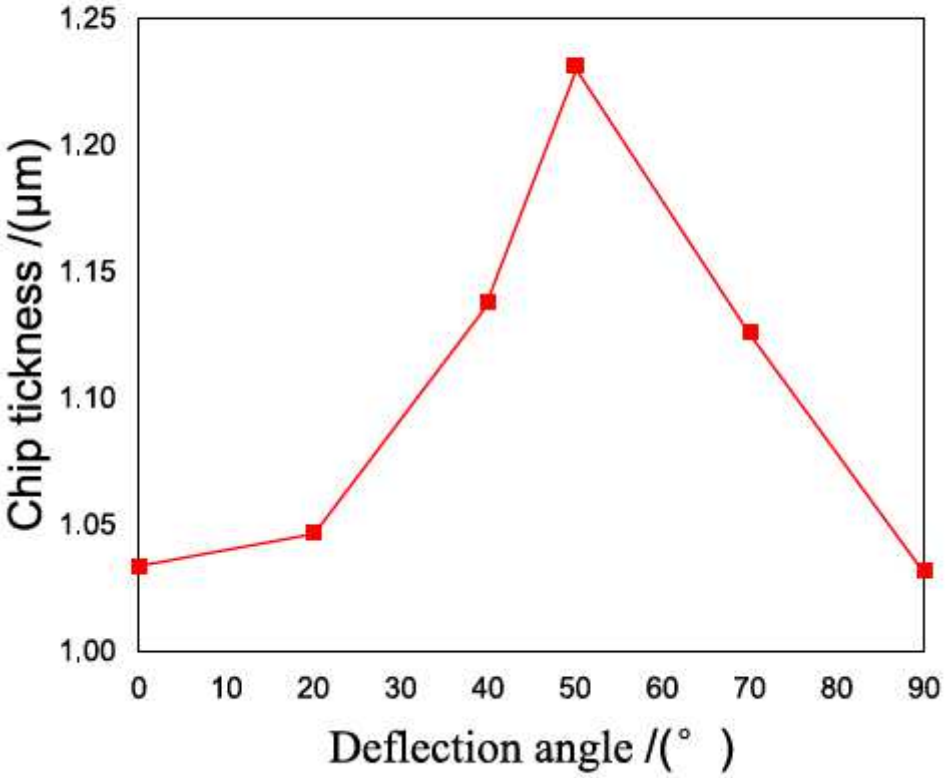

(b) The chip thickness of the UEVC with varied deflection angle

Figure 14

Simulation of the chips of the UEVC with varied deflection angle

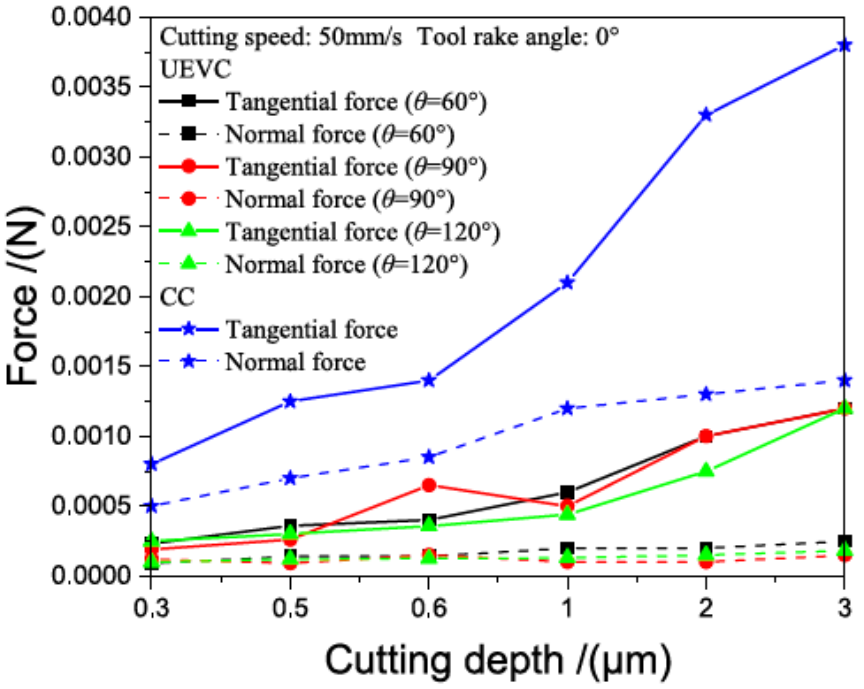

(a) Relationship of cutting depth and cutting force

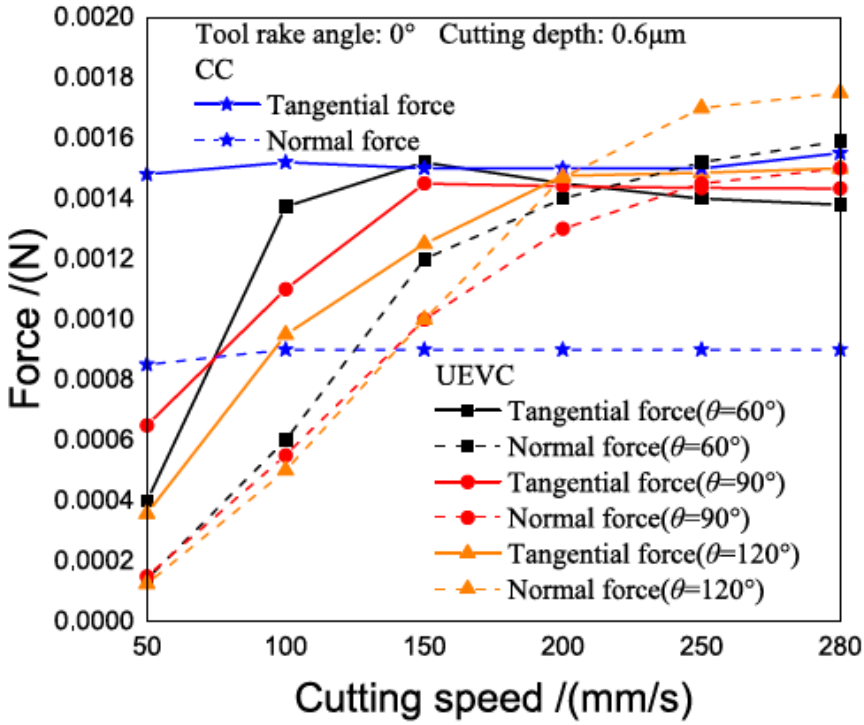

(b) Relationship of cutting speed and cutting force

Figure 15

Comparison of cutting forces between UEVC and CC at different cutting depths and speeds

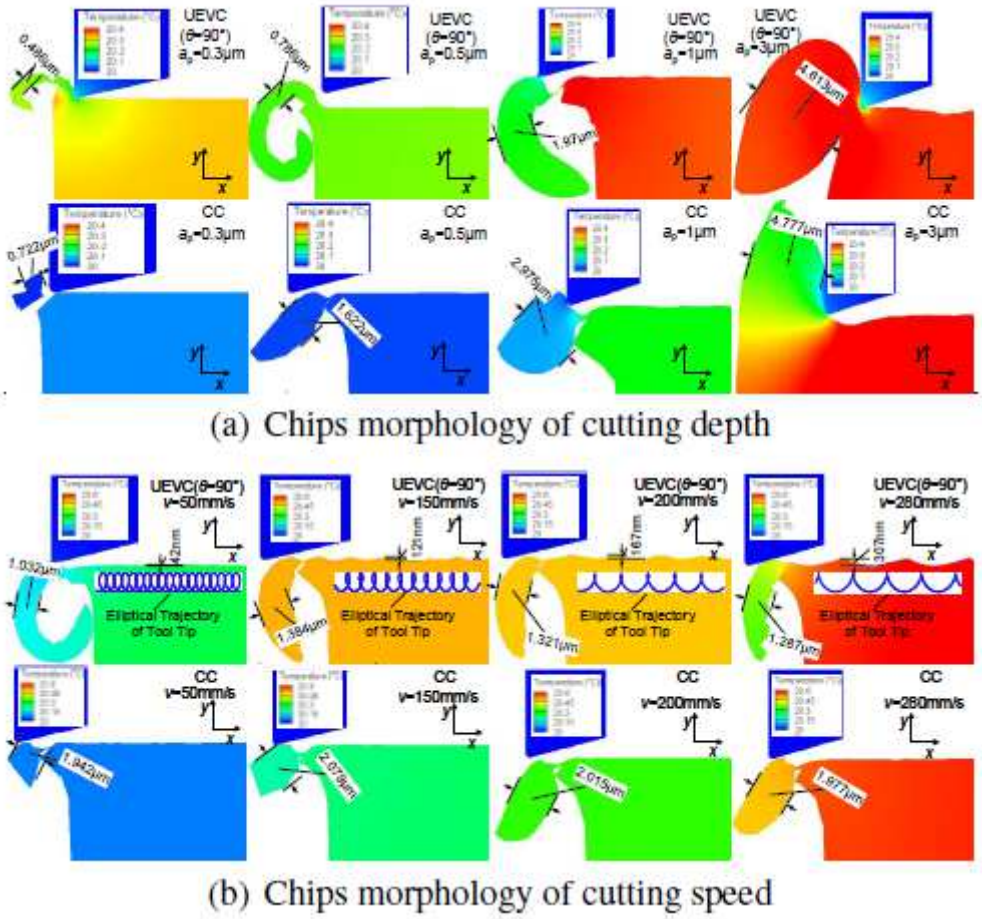

(a) Chips morphology of cutting depth

(b) Chips morphology of cutting speed

Figure 16

Comparative analysis of chips between UEVC and CC at different cutting depths and speeds

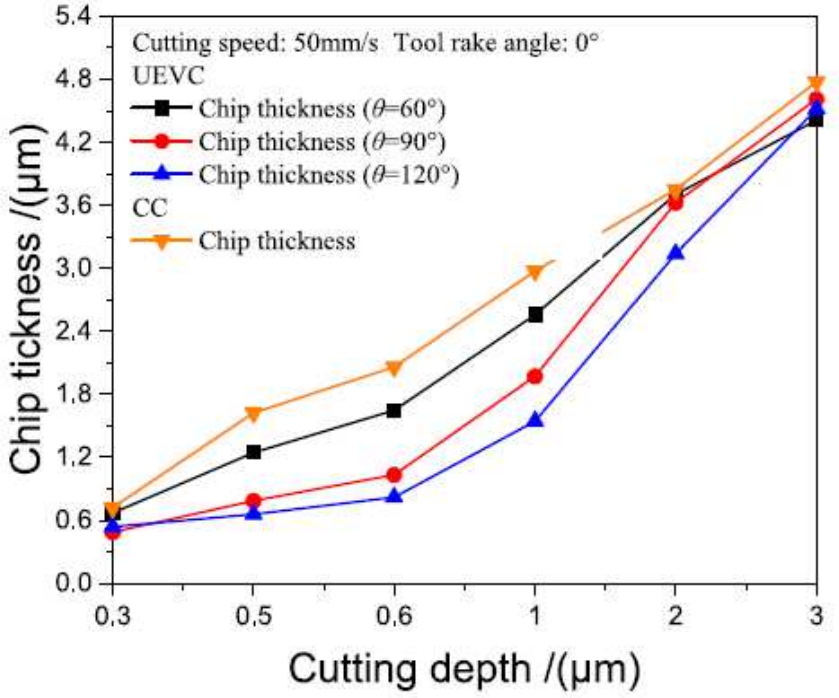

(a) Relationship between cutting depth and chip thickness

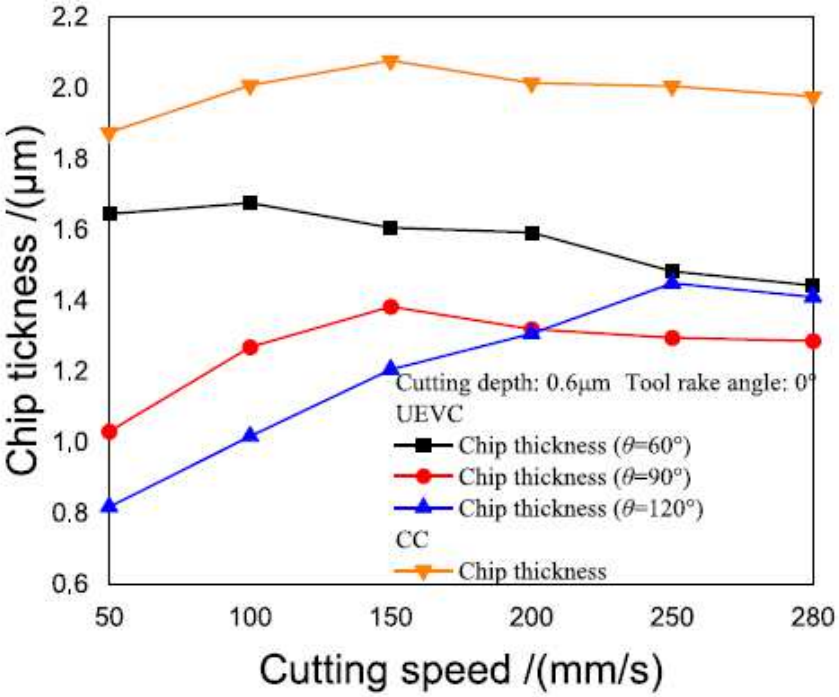

(b) Relationship between cutting speed and chip thickness

Figure 17

Comparison of chip thickness between UEVC and CC at different cutting depths and speeds

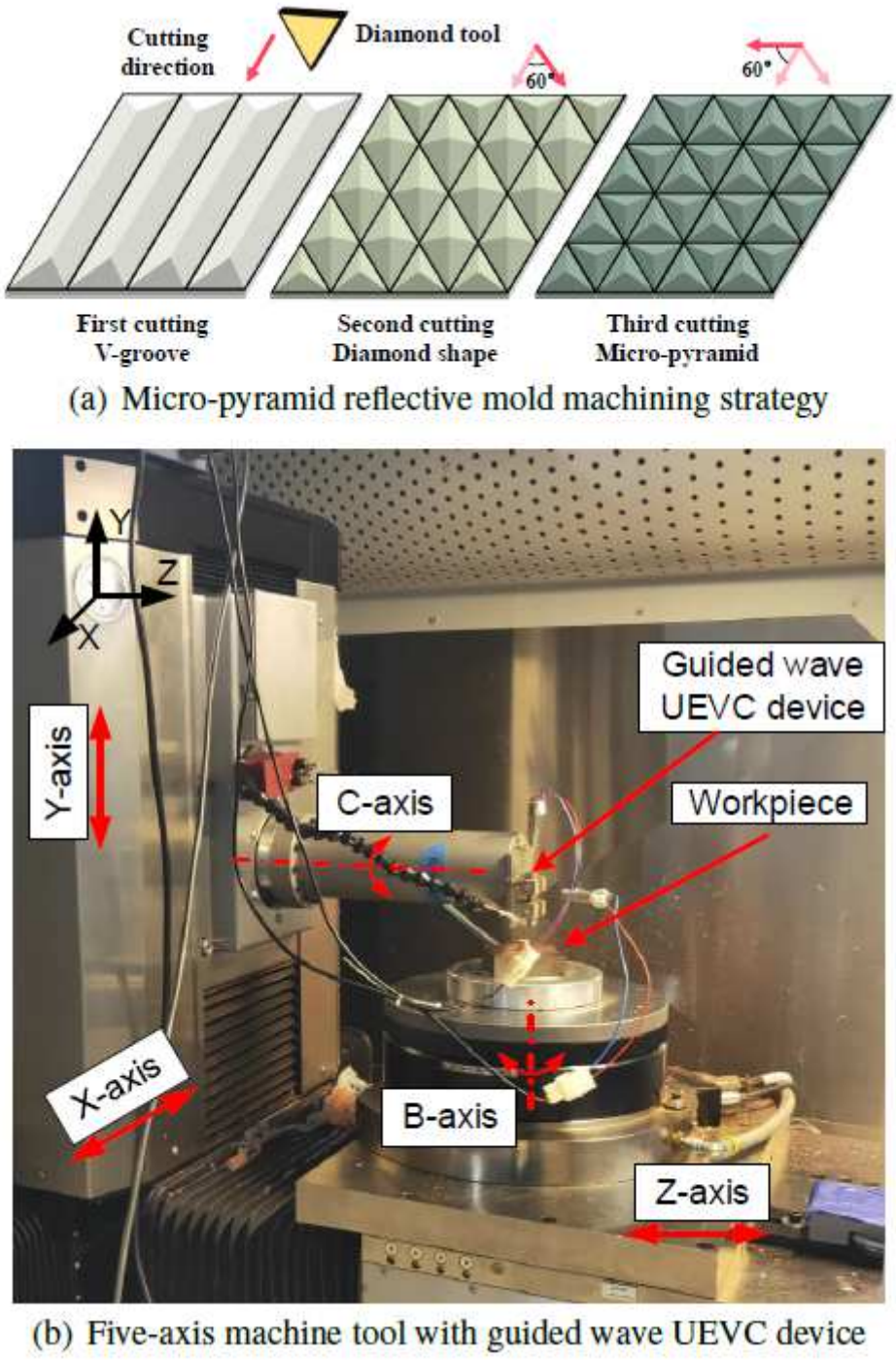

Figure 18

Five-axis ultra-precision machine tool and micro-pyramid reflective mold machining strategy

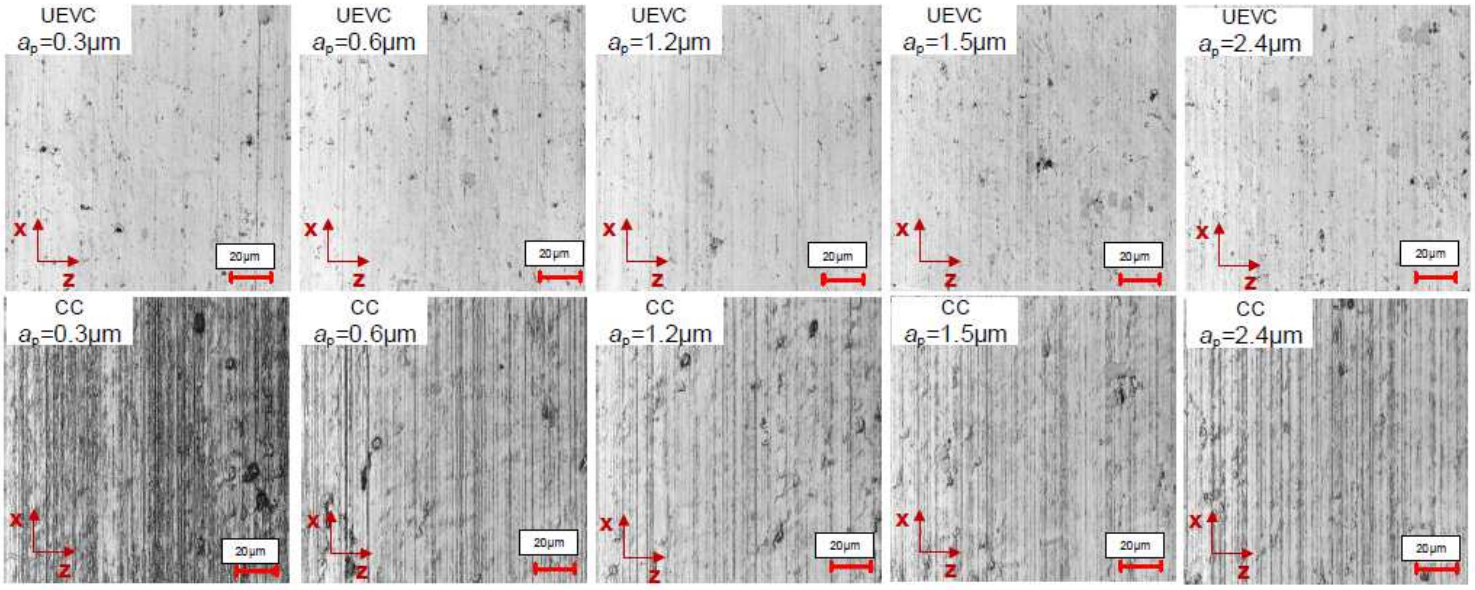

(a) Surface morphology of UEVC and CC plane machining

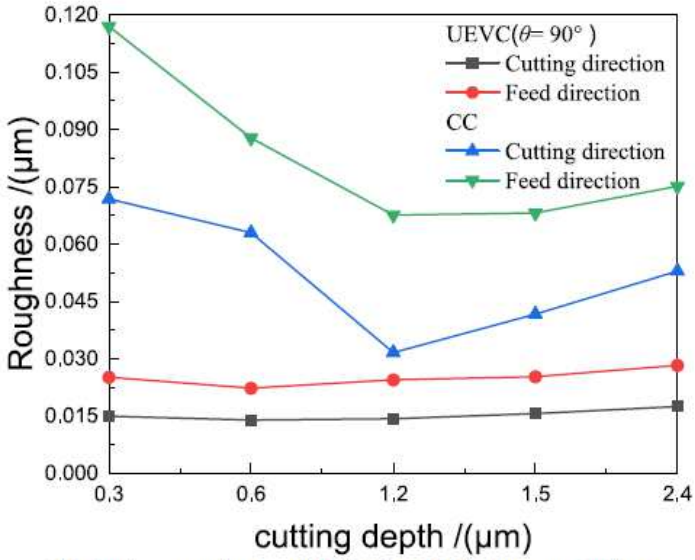

(b) Surface roughness of UEVC and CC plane machining

Figure 19

Comparison of UEVC and CC plane machining under varied cutting depths

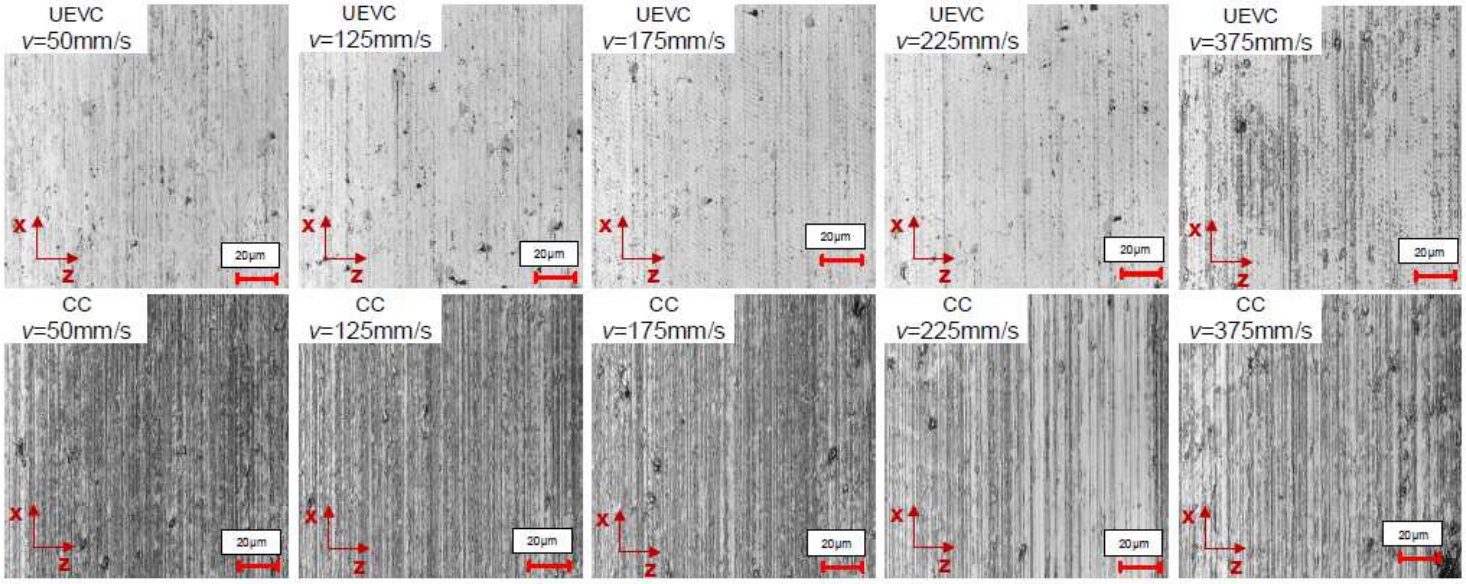

(a) Surface morphology of UEVC and CC

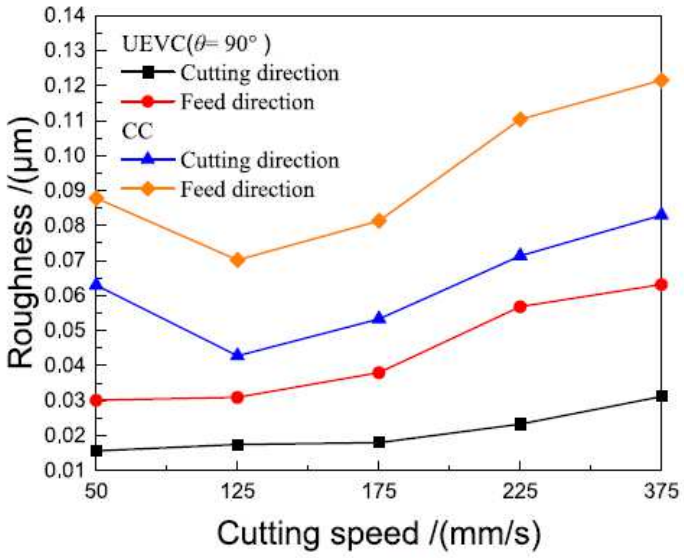

(b) Surface roughness of UEVC and CC

Figure 20

Comparison of UEVC and CC plane machining under varied cutting speed

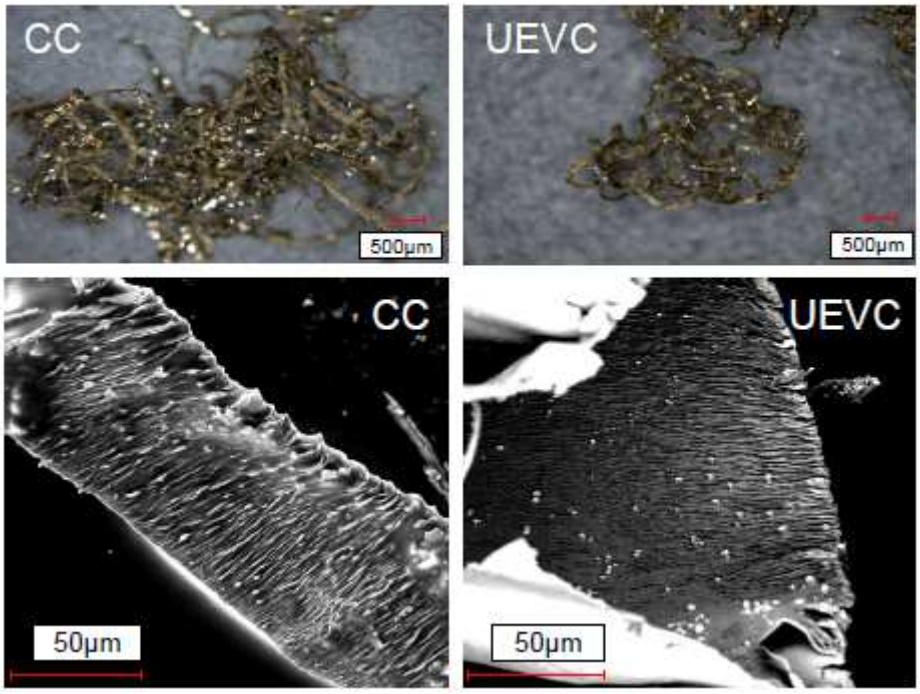

Figure 21

The elliptic trajectory of the guided wave UEVC device

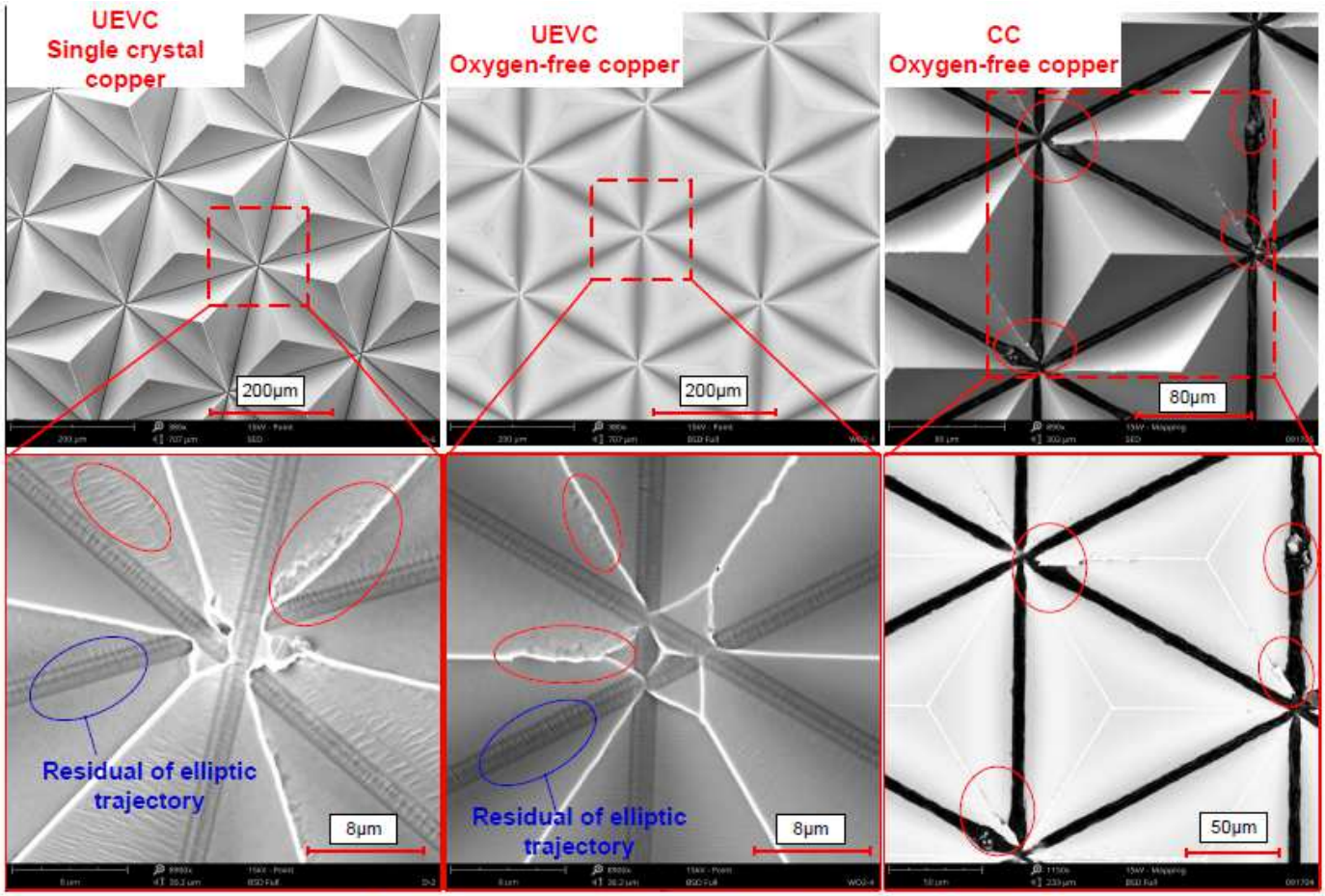

(a) SEM test of the micro-pyramid array machined in guided wave UEVC and CC

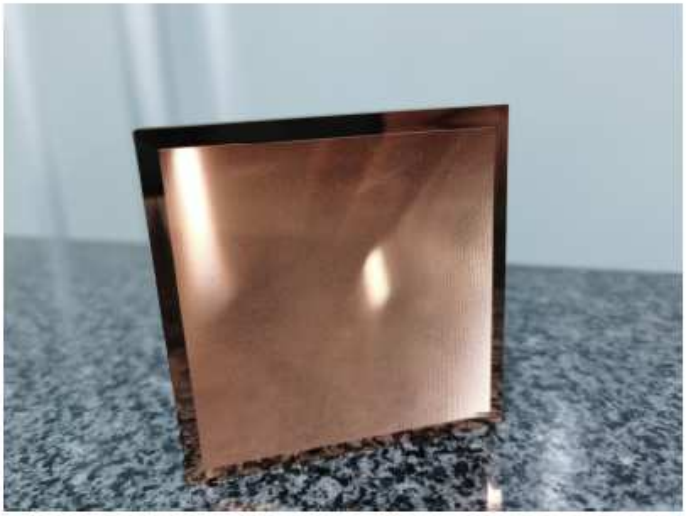

(b) Micro-pyramid reflective mold with guided wave UEVC

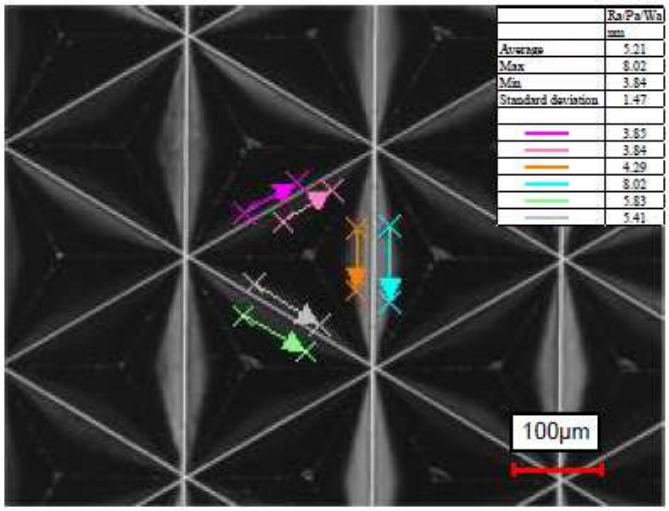

(c) Surface roughness of the micro-pyramid element

Figure 22

The cutting experiment of the micro-pyramid reflective mold in guided wave UEVC and CC